bioRxiv preprint doi: https://doi.org/10.1101/2021.12.07.470392; this version posted December 22, 2021. The copyright holder for this preprint (which was not certified by peer review) is the author/funder. All rights reserved. No reuse allowed without permission.

Omicron escapes the majority of existing SARS-CoV-2 neutralizing antibodies

Yunlong Cao[1,2,#,*], Jing Wang[1,3,#], Fanchong Jian[1,4,#], Tianhe Xiao[1,5,#], Weiliang Song[1,3,#], Ayijiang Yisimayi[1,3,#], Weijin Huang[6,#], Qianqian Li[6], Peng Wang[1], Ran An[1], Jing Wang[1], Yao Wang[1], Xiao Niu[1,4], Sijie Yang[1,7], Hui Liang[1], Haiyan Sun[1], Tao Li[6], Yuanling Yu[6], Qianqian Cui[6], Shuo Liu[6], Xiaodong Yang[8], Shuo Du[3], Zhiying Zhang[3], Xiaohua Hao[9], Fei Shao[1], Ronghua Jin[9], Xiangxi Wang[10,*], Junyu Xiao[2,3,*], Youchun Wang[6,*], Xiaoliang Sunney Xie[1,2,*]

[1]Biomedical Pioneering Innovation Center (BIOPIC), Peking University, Beijing, P.R. China.

[2]Beijing Advanced Innovation Center for Genomics (ICG), Peking University, Beijing, P.R. China.

[3]School of Life Sciences, Peking University, Beijing, P.R. China.

[4]College of Chemistry and Molecular Engineering, Peking University, Beijing, P.R. China.

[5]Joint Graduate Program of Peking-Tsinghua-NIBS, Academy for Advanced Interdisciplinary Studies, Peking University, Beijing, China.

[6]Division of HIV/AIDS and Sex-transmitted Virus Vaccines, Institute for Biological Product Control, National Institutes for Food and Drug Control (NIFDC), Beijing, P.R. China.

[7]Tsinghua-Peking Center for Life Sciences, Beijing, P.R. China.

[8]Beijing YouAn Hospital, Capital Medical University, Beijing, P.R. China.

[9]Beijing Ditan Hospital, Capital Medical University, Beijing, P.R. China.

[10]CAS Key Laboratory of Infection and Immunity, National Laboratory of Macromolecules, Institute of Biophysics, Chinese Academy of Sciences, Beijing, P.R. China.

[*]Correspondence: Yunlong Cao (yunlongcao@pku.edu.cn); Junyu Xiao (junyuxiao@pku.edu.cn); Xiangxi Wang (xiangxi@ibp.ac.cn); Youchun Wang (wangyc@nifdc.org.cn); Xiaoliang Sunney Xie (sunneyxie@biopic.pku.edu.cn)

[#]These authors contributed equally.

Abstract

bioRxiv preprint doi: https://doi.org/10.1101/2021.12.07.470392; this version posted December 22, 2021. The copyright holder for this preprint (which was not certified by peer review) is the author/funder. All rights reserved. No reuse allowed without permission.

The SARS-CoV-2 B.1.1.529 variant (Omicron) contains 15 mutations on the receptor-binding domain (RBD). How Omicron would evade RBD neutralizing antibodies (NAbs) requires immediate investigation. Here, we used high-throughput yeast display screening[1,2] to determine the RBD escaping mutation profiles for 247 human anti-RBD NAbs and showed that the NAbs could be unsupervised clustered into six epitope groups (A-F), which is highly concordant with knowledge-based structural classifications[3-5]. Strikingly, various single mutations of Omicron could impair NAbs of different epitope groups. Specifically, NAbs in Group A-D, whose epitope overlap with ACE2-binding motif, are largely escaped by K417N, G446S, E484A, and Q493R. Group E (S309 site)[6] and F (CR3022 site)[7] NAbs, which often exhibit broad sarbecovirus neutralizing activity, are less affected by Omicron, but still, a subset of NAbs are escaped by G339D, N440K, and S371L. Furthermore, Omicron pseudovirus neutralization showed that single mutation tolerating NAbs could also be escaped due to multiple synergetic mutations on their epitopes. In total, over 85% of the tested NAbs are escaped by Omicron. Regarding NAb drugs, the neutralization potency of LY-CoV016/LY-CoV555, REGN10933/REGN10987, AZD1061/AZD8895, and BRII-196 were greatly reduced by Omicron, while VIR-7831 and DXP-604 still function at reduced efficacy. Together, data suggest Omicron would cause significant humoral immune evasion, while NAbs targeting the sarbecovirus conserved region remain most effective. Our results offer instructions for developing NAb drugs and vaccines against Omicron and future variants.

bioRxiv preprint doi: https://doi.org/10.1101/2021.12.07.470392; this version posted December 22, 2021. The copyright holder for this preprint (which was not certified by peer review) is the author/funder. All rights reserved. No reuse allowed without permission.

Main

The severe acute respiratory syndrome coronavirus 2 (SARS-CoV-2) variant B.1.1.529 was first reported to the World Health Organization (WHO) on 24 November 2021. It appears to be rapidly spreading, and the WHO classified it as a variant of concern (VOC) only two days after, designating it as Omicron [8,9]. An unusually large number of mutations are found in Omicron, including over 30 in the spike protein (Extended Data Fig. 1a). The receptor-binding domain, responsible for interacting with the Angiotensin-Converting Enzyme 2 (ACE2) receptor, bears 15 of these mutations, including G339D, S371L, S373P, S375F, K417N, N440K, G446S, S477N, T478K, E484A, Q493R, G496S, Q498R, N501Y, and Y505H. Some of these mutations are very concerning due to their well-understood functional consequences, such as K417N and N501Y, which contribute to immune escape and higher infectivity [10-13]. Many other mutations' functional impacts remain to be investigated.

The S protein is the target of essentially all NAbs found in the convalescent sera or elicited by vaccines. Most of the N-terminal domain (NTD) neutralizing antibodies target an antigenic "supersite" in NTD, involving the N3 (residues 141 to 156) and N5 (residues 246 to 260) loops [14,15], and are thus very prone to NTD mutations. Omicron carries the Δ143-145 mutation, which would alter the N3 loop and most likely result in immune escape of most anti-NTD NAbs (Extended Data Fig. 1b). Compared to NTD targeting NAbs, RBD targeting NAbs are particularly abundant and potent, and display diverse epitopes. Evaluating how Omicron affects the neutralization capability of anti-RBD NAbs of diverse classes and epitopes is urgently needed.

RBD-directed SARS-CoV-2 NAbs can be assigned into different classes or binding sites based on structural analyses by cryo-EM or high-resolution crystallography [3-5]; however, structural data only indicates the contacting amino acids, but does not infer the escaping mutations for a specific antibody. Recent advances in deep antigen mutation screening using FACS (fluorescence-activated cell sorting)-based yeast display platform has allowed the quick mapping of all single amino acid mutations in the RBD that affect the binding of SARS-CoV-2 RBD NAbs [1,16]. The method has proven highly effective in predicting NAB drug efficacy toward mutations [2]. However, to study how human humoral immunity may react to highly mutated variants like

bioRxiv preprint doi: https://doi.org/10.1101/2021.12.07.470392; this version posted December 22, 2021. The copyright holder for this preprint (which was not certified by peer review) is the author/funder. All rights reserved. No reuse allowed without permission.

Omicron requires mutation profiling of a large collection of NAbs targeting different regions of RBD, and FACS-based yeast display mutation screening is limited by low experimental throughput. Here we further developed a MACS (magnetic-activated cell sorting) -based screening method which increases the throughput near 100-fold and could obtain comparable data quality like FACS (Fig 1a, Extended Data Fig. 2). Using this method, we quickly characterized the RBD escaping mutation profile for a total of 247 NAbs (Supplementary Data 1). Half of the NAbs were part of the antibodies identified by us using single-cell VDJ sequencing of antigen-specific memory B cells from SARS-CoV-2 convalescents, SARS-CoV-2 vaccinees, and SARS-CoV-1 convalescents who recently received SARS-CoV-2 vaccines (Supplementary Data 2). The other half of NAbs were identified by groups worldwide [3,5,6,11,17-40] (Supplementary Table 1).

The high-throughput screening capability allowed us to classify these NAbs into six Epitope Groups (A-F) using unsupervised clustering without dependence on structural studies, and the grouping is highly concordant with the knowledge-based structural classifications [3-5] (Fig. 1b, c). In particular, Group A-D NAbs largely correspond to the RBS A-D NAbs described by Yuan et al. [4] and overlap with the class 1-2 NAbs described by Barnes et al. [3] in general. The epitopes of these NAbs largely overlap with RBD residues involved in the binding to ACE2. Group A and B NAbs, represented by LY-CoV016 and AZD8895, respectively, usually can only bind to the 'up' RBD; whereas most of the Group C and D members, such as LY-CoV555 and REGN-10987, bind to RBDs regardless of their 'up' and 'down' conformations. Group E and F NAbs are very similar to the class 3 and 4 NAbs described by Barnes et al. [3] and target the S309/VIR-7831 site and CR3022 site, which could exhibit pan-sarbecovirus neutralization capacity (Fig 1e). Most of these NAbs neutralize SARS-CoV-2 using mechanisms other than directly interfering with ACE2 binding.

Inferred from the escaping mutation profiles, various single mutations of Omicron could impair NAbs of different epitope groups (Extended Data Fig. 3). Specifically, NAbs in Group A-D, whose epitope overlaps with ACE2-binding motif, are largely escaped by single mutations of K417N, G446S, E484A, and Q493R. Also, a subset of NAbs of Group E and F are escaped by single mutations of G339D, N440K, S371L, S375F. However, due to the extensive mutations accumulated on Omicron's RBD,

bioRxiv preprint doi: https://doi.org/10.1101/2021.12.07.470392; this version posted December 22, 2021. The copyright holder for this preprint (which was not certified by peer review) is the author/funder. All rights reserved. No reuse allowed without permission.

studying NAb's response to Omicron only in the single mutation context is insufficient. Indeed, Omicron pseudovirus neutralization and spike enzyme-linked immunosorbent assay (ELISA) showed that single mutation tolerating NAbs could also be escaped by Omicron due to multiple synergetic mutations on their epitopes (Fig 1d, Extended Data Fig. 3). In total, over 85% of the tested human NAbs are escaped, suggesting that Omicron could cause significant humoral immune evasion and potential antigenic shifting.

It is crucial to analyze how each group of NAbs reacts to Omicron to instruct the development of NAb drugs and vaccines. Group A NAbs mainly contains the *VH3-53/VH3-66* germline gene-encoded antibodies, which are abundantly present in our current collection of SARS-CoV-2 neutralizing antibodies [17,21,22,26,41-43], including several antibodies that have obtained emergency use authorization (CB6/LY-CoV016) [19] or are currently being studied in clinical trials (P2C-1F11/BRII-196, BD-604/DXP-604) [18,44] (Fig. 2a, Extended Data Fig. 4a). Group A NAbs often exhibit less somatic mutations and shorter CDR3 length compared to other groups (Extended Data Fig. 5a, b). The epitopes of these antibodies extensively overlap with the binding site of ACE2 and are often evaded by RBD mutations on K417, D420, F456, A475, L455 sites (Fig 2d, Extended Data Fig. 6a,7a). Most NAbs in Group A were already escaped by B.1.351 (Beta) strain (Extended Data Fig. 5d), specifically by K417N (Extended Data Fig. 8a), due to a critical salt bridge interaction between Lys417 and a negatively charged residue in the antibody (Fig. 2g). The NAbs that survived Beta strain, such as BRII-196 and DXP-604, are insensitive to the K417N single site change but could also be heavily affected by the combination of K417N and other RBD mutations located on their epitopes, like S477N, Q493R, G496S, Q498R, N501Y, and Y505H of Omicron, causing lost or reduction of neutralization (Fig 2d; Extended Data Fig. 7a).

The *VH1-58* gene-encoded NAbs are enriched in Group B (Extended Data Fig. 4b). These NAbs such as AZD8895 [36], REGN-10933 [42], and BD-836 [45] bind to the left shoulder of RBD, often focusing on the far tip (Fig. 2h). These NAbs are very sensitive to the change of F486, N487, and G476 (Fig 2b, Extended Data Fig. 6b). Fortunately, F486 and a few other major targeting sites of these NAbs are critically involved in ACE2-binding, and therefore they are generally harder to be escaped. A subset of NAbs in Group B, such as AZD8895 and BD-836, could survive Beta (Fig 2e); however,

bioRxiv preprint doi: https://doi.org/10.1101/2021.12.07.470392; this version posted December 22, 2021. The copyright holder for this preprint (which was not certified by peer review) is the author/funder. All rights reserved. No reuse allowed without permission.

Omicron significantly reduced Group B NAbs' binding affinity to RBD, potentially through S477N/T478K/E484A on their epitope (Extended Data Fig. 7b) [46], resulting in the loss of neutralization.

Group C NAbs are frequently encoded by *VH1-2* and *VH1-69* (Extended Data Fig. 4c). The majority of NAbs in this group could bind to both "up" and "down" RBDs, resulting in higher neutralization potency compared to other groups (Fig. 2c, Extended Data Fig. 5c). Several highly potent antibodies are found in Group C, including BD-368-2/DXP-593 [44], C002 [3], and LY-CoV555 [47]. They bind to the right shoulder of RBD (Fig. 2i), and are mostly prone to the change of E484 (Extended Data Fig. 6c, 7c), such as the E484K mutation found in Beta (Fig. 2f). The E484A mutation seen in Omicron elicited a similar escaping effect, although the change to Ala is slightly subtler, and could be tolerated by certain antibodies in this group (Extended Data Fig. 8b). All Group C NAbs tested are escaped by Omicron.

Group D NAbs consist of diverse IGHV gene-encoded antibodies (Extended Data Fig. 4d). Prominent members in this group include REGN-10987 [42] and AZD1061 [36] (Fig. 3a). They further rotate down from the RBD right shoulder towards the S309 site when compared to Group C NAbs (Fig. 3g). As a loop formed by residues 440-449 in RBD is critical for the targeting of this group of NAbs, they are sensitive to the changes of N440, K444, G446, and N448 (Extended Data Fig. 6d, 7d). Most NAbs of Group D remain active against Beta; however, G446S would substantially affect their neutralization capability against Omicron (Fig. 3d). Also, for those NAbs that could tolerate G446S single mutation, the N440K/G446S combination may significantly reduce their binding affinity, resulting in that most Group D NAbs are escaped by Omicron.

Group E and F NAbs are rarer when compared to the other four groups. The archetypical member of each group was originally isolated from a SARS-CoV-1 convalescent, and displays SARS-CoV-2 cross-neutralizing activity. There is no clear VDJ convergent effect compared to Group A, B, and C (Extended Data Fig. 4e, f), and the mutation rate and CDR3 length are larger than other groups. NAbs in Group E and F rarely compete with ACE2; thus, their average half-maximal inhibitory concentration (IC50) is higher than NAbs in Group A-D (Extended Data Fig. 5c). NAbs in Group E,

bioRxiv preprint doi: https://doi.org/10.1101/2021.12.07.470392; this version posted December 22, 2021. The copyright holder for this preprint (which was not certified by peer review) is the author/funder. All rights reserved. No reuse allowed without permission.

193 such as VIR-7831/S309, may recognize a mixed protein/carbohydrate epitope,
194 involving the N-linked glycan on N343 [6] (Fig. 3h). Inferred from the escaping mutation
195 profiles (Fig. 3b), Group E NAbs are often sensitive to changes of G339, T345, and
196 R346 (Extended Data Fig 6e, 7e). The G339D mutation would affect a subset of NAbs'
197 neutralization performance (Fig. 3e). Also, part of Group E NAbs' epitope would
198 extend to the 440-449 loop, making them sensitive to N440K in Omicron (Fig. 3e).
199 Noticeably, the population of Omicron with R346K is continuously increasing, which
200 may severely affect the neutralization capacity of Group E NAbs.
201
202 Group F NAbs such as S304 target a cryptic site in RBD that is generally not exposed
203 (Fig. 3i), therefore their neutralizing activities are generally weaker [7]. Group F NAbs
204 are often sensitive to changes of F374, T376, and K378 (Extended Data Fig. 6f, 7f). A
205 loop involving RBD residues 371-375 lies in the ridge between the E and F sites;
206 therefore, a subset of Group F NAbs, including some Group E NAbs, could be affected
207 by the S371L/S373P/S375F mutations if their epitopes extend to this region (Fig. 3c,
208 f). Interestingly, a part of Group F NAbs is highly sensitive to V503 and G504, similar
209 to the epitopes of S2X259 (Fig. 3f, j), suggesting that they can compete with ACE2.
210 Indeed, several NAbs, such as BD55-5300 and BD55-3372, exhibit higher
211 neutralization potency than other NAbs in Group F (Fig. 3c, 4b). However, These
212 antibodies' neutralization capability might be undermined by N501Y and Y505H of
213 Omicron (Fig. 3j).
214
215 As for NAb drugs, consistent with their escaping mutation profiles, the neutralization
216 potency of LY-CoV016/LY-CoV555, REGN-10933/REGN-10987, and AZD1061 are
217 greatly reduced by Omicron (Fig. 4a, Extended Data Fig. 9). The binding affinity of
218 AZD8895 and BRII-196 toward Omicron RBD is also significantly reduced, likely due
219 to multiple mutations accumulating on their epitopes, such that AZD8895 and BRII-
220 196 failed to neutralize Omicron (Extended Data Fig. 10). BRII-198 was not tested
221 since the antibody sequence was not released. VIR-7831 retains strong RBD binding
222 capability, although G339 is part of its epitope, the G339D mutation in Omicron does
223 not appear to affect VIR-7831's binding; however, VIR-7831's IC50 is reduced to 181
224 ng/mL, and may be subject to further reduction against Omicron with R346K. DXP-
225 604's binding affinity against Omicron RBD is largely reduced compared to wildtype
226 RBD; nevertheless, it can still neutralize Omicron at an IC50 of 287 ng/mL, a nearly

bioRxiv preprint doi: https://doi.org/10.1101/2021.12.07.470392; this version posted December 22, 2021. The copyright holder for this preprint (which was not certified by peer review) is the author/funder. All rights reserved. No reuse allowed without permission.

30-fold reduction compared to wildtype (Fig. 4a). Additionally, several NAbs in Group E and F have shown high potency against Omicron and broad pan-sarbecovirus neutralization ability, promising for NAb drug development (Fig. 4b). Many more NAbs identified from vaccinated SARS-CoV-1 convalescents are waiting to be characterized.

The high-throughput yeast screening method provides a laboratory means for quickly examining the epitope of a certain NAb; however, the current throughput using FACS is limited and can not be used to evaluate a large NAb library. By virtue of MACS, we are able to increase the throughput by two orders of magnitude. In doing so, we were able to gain statistical confidence for the survival proportion of anti-RBD NAbs in each epitope group against Omicron. The experimental accuracy for predicting the neutralization reduction for single amino acid mutations is relatively high (Extended Data Fig. 8a, b); however, current mutation screening through yeast display could not effectively probe the consequence of multiple mutations simultaneously, which requires further technical optimization.

To date, a large number of SARS-CoV-2 anti-RBD NAbs have been identified from convalescents and vaccinees. The most potent NAbs are frequently found in Groups A-D as we described above, which tend to directly interfere with the binding of ACE2. Nevertheless, the neutralizing powers of these NAbs are often abrogated by RBD mutations in the evolutionary arms race between SARS-CoV-2 and human humoral immunity. Indeed, we showed that Omicron would escape the majority of SARS-CoV-2 NAbs in this collection (Extended Data Fig. 5e). On the other hand, Groups E and F NAbs are less affected by Omicron, likely because they are not abundant in population [48], hence exerting less evolutionary pressure for RBD to mutate in the corresponding epitope groups. These NAbs target conserved RBD regions in sarbecovirus and therefore are ideal targets for future development of pan-sarbecovirus NAb drugs.

References

1 Starr, T. N. *et al.* Prospective mapping of viral mutations that escape antibodies used to treat COVID-19. *Science* **371**, 850-854, doi:10.1126/science.abf9302 (2021).

2 Starr, T. N., Greaney, A. J., Dingens, A. S. & Bloom, J. D. Complete map of SARS-CoV-2 RBD mutations that escape the monoclonal antibody LY-

bioRxiv preprint doi: https://doi.org/10.1101/2021.12.07.470392; this version posted December 22, 2021. The copyright holder for this preprint (which was not certified by peer review) is the author/funder. All rights reserved. No reuse allowed without permission.

CoV555 and its cocktail with LY-CoV016. *Cell Rep Med* **2**, 100255, doi:10.1016/j.xcrm.2021.100255 (2021).

3 Barnes, C. O. *et al.* SARS-CoV-2 neutralizing antibody structures inform therapeutic strategies. *Nature* **588**, 682-687, doi:10.1038/s41586-020-2852-1 (2020).

4 Yuan, M. *et al.* Structural and functional ramifications of antigenic drift in recent SARS-CoV-2 variants. *Science* **373**, 818-823, doi:10.1126/science.abh1139 (2021).

5 Dejnirattisai, W. *et al.* The antigenic anatomy of SARS-CoV-2 receptor binding domain. *Cell* **184**, 2183-2200 e2122, doi:10.1016/j.cell.2021.02.032 (2021).

6 Pinto, D. *et al.* Cross-neutralization of SARS-CoV-2 by a human monoclonal SARS-CoV antibody. *Nature* **583**, 290-295, doi:10.1038/s41586-020-2349-y (2020).

7 Yuan, M. *et al.* A highly conserved cryptic epitope in the receptor binding domains of SARS-CoV-2 and SARS-CoV. *Science* **368**, 630-633, doi:10.1126/science.abb7269 (2020).

8 Callaway, E. Heavily mutated Omicron variant puts scientists on alert. *Nature* **600**, 21, doi:10.1038/d41586-021-03552-w (2021).

9 Callaway, E. & Ledford, H. How bad is Omicron? What scientists know so far. *Nature*, doi:10.1038/d41586-021-03614-z (2021).

10 Li, Q. *et al.* SARS-CoV-2 501Y.V2 variants lack higher infectivity but do have immune escape. *Cell* **184**, 2362-2371 e2369, doi:10.1016/j.cell.2021.02.042 (2021).

11 Cao, Y. *et al.* Humoral immune response to circulating SARS-CoV-2 variants elicited by inactivated and RBD-subunit vaccines. *Cell Res* **31**, 732-741, doi:10.1038/s41422-021-00514-9 (2021).

12 Starr, T. N. *et al.* Deep Mutational Scanning of SARS-CoV-2 Receptor Binding Domain Reveals Constraints on Folding and ACE2 Binding. *Cell* **182**, 1295-1310 e1220, doi:10.1016/j.cell.2020.08.012 (2020).

13 Gu, H. *et al.* Adaptation of SARS-CoV-2 in BALB/c mice for testing vaccine efficacy. *Science* **369**, 1603-1607, doi:10.1126/science.abc4730 (2020).

14 Cerutti, G. *et al.* Potent SARS-CoV-2 neutralizing antibodies directed against spike N-terminal domain target a single supersite. *Cell Host Microbe* **29**, 819-833 e817, doi:10.1016/j.chom.2021.03.005 (2021).

15 McCallum, M. *et al.* N-terminal domain antigenic mapping reveals a site of vulnerability for SARS-CoV-2. *Cell* **184**, 2332-2347 e2316, doi:10.1016/j.cell.2021.03.028 (2021).

16 Greaney, A. J. *et al.* Complete Mapping of Mutations to the SARS-CoV-2 Spike Receptor-Binding Domain that Escape Antibody Recognition. *Cell Host Microbe* **29**, 44-57 e49, doi:10.1016/j.chom.2020.11.007 (2021).

17 Cao, Y. *et al.* Potent Neutralizing Antibodies against SARS-CoV-2 Identified by High-Throughput Single-Cell Sequencing of Convalescent Patients' B Cells. *Cell* **182**, 73-84 e16, doi:10.1016/j.cell.2020.05.025 (2020).

18 Ju, B. *et al.* Human neutralizing antibodies elicited by SARS-CoV-2 infection. *Nature* **584**, 115-119, doi:10.1038/s41586-020-2380-z (2020).

19 Shi, R. *et al.* A human neutralizing antibody targets the receptor-binding site of SARS-CoV-2. *Nature* **584**, 120-124, doi:10.1038/s41586-020-2381-y (2020).

bioRxiv preprint doi: https://doi.org/10.1101/2021.12.07.470392; this version posted December 22, 2021. The copyright holder for this preprint (which was not certified by peer review) is the author/funder. All rights reserved. No reuse allowed without permission.

20 Wu, Y. *et al.* A noncompeting pair of human neutralizing antibodies block COVID-19 virus binding to its receptor ACE2. *Science* **368**, 1274-1278, doi:10.1126/science.abc2241 (2020).

21 Yuan, M. *et al.* Structural basis of a shared antibody response to SARS-CoV-2. *Science* **369**, 1119-1123, doi:10.1126/science.abd2321 (2020).

22 Robbiani, D. F. *et al.* Convergent antibody responses to SARS-CoV-2 in convalescent individuals. *Nature* **584**, 437-442, doi:10.1038/s41586-020-2456-9 (2020).

23 Liu, L. *et al.* Potent neutralizing antibodies against multiple epitopes on SARS-CoV-2 spike. *Nature* **584**, 450-456, doi:10.1038/s41586-020-2571-7 (2020).

24 Baum, A. *et al.* Antibody cocktail to SARS-CoV-2 spike protein prevents rapid mutational escape seen with individual antibodies. *Science* **369**, 1014-1018, doi:10.1126/science.abd0831 (2020).

25 Brouwer, P. J. M. *et al.* Potent neutralizing antibodies from COVID-19 patients define multiple targets of vulnerability. *Science* **369**, 643-650, doi:10.1126/science.abc5902 (2020).

26 Rogers, T. F. *et al.* Isolation of potent SARS-CoV-2 neutralizing antibodies and protection from disease in a small animal model. *Science* **369**, 956-963, doi:10.1126/science.abc7520 (2020).

27 Piccoli, L. *et al.* Mapping Neutralizing and Immunodominant Sites on the SARS-CoV-2 Spike Receptor-Binding Domain by Structure-Guided High-Resolution Serology. *Cell* **183**, 1024-1042 e1021, doi:10.1016/j.cell.2020.09.037 (2020).

28 Zost, S. J. *et al.* Potently neutralizing and protective human antibodies against SARS-CoV-2. *Nature* **584**, 443-449, doi:10.1038/s41586-020-2548-6 (2020).

29 Tortorici, M. A. *et al.* Ultrapotent human antibodies protect against SARS-CoV-2 challenge via multiple mechanisms. *Science* **370**, 950-957, doi:10.1126/science.abe3354 (2020).

30 Lv, Z. *et al.* Structural basis for neutralization of SARS-CoV-2 and SARS-CoV by a potent therapeutic antibody. *Science* **369**, 1505-1509, doi:10.1126/science.abc5881 (2020).

31 Zost, S. J. *et al.* Rapid isolation and profiling of a diverse panel of human monoclonal antibodies targeting the SARS-CoV-2 spike protein. *Nat Med* **26**, 1422-1427, doi:10.1038/s41591-020-0998-x (2020).

32 Seydoux, E. *et al.* Analysis of a SARS-CoV-2-Infected Individual Reveals Development of Potent Neutralizing Antibodies with Limited Somatic Mutation. *Immunity* **53**, 98-105 e105, doi:10.1016/j.immuni.2020.06.001 (2020).

33 Kreye, J. *et al.* A Therapeutic Non-self-reactive SARS-CoV-2 Antibody Protects from Lung Pathology in a COVID-19 Hamster Model. *Cell* **183**, 1058-1069 e1019, doi:10.1016/j.cell.2020.09.049 (2020).

34 Scheid, J. F. *et al.* B cell genomics behind cross-neutralization of SARS-CoV-2 variants and SARS-CoV. *Cell* **184**, 3205-3221 e3224, doi:10.1016/j.cell.2021.04.032 (2021).

35 Tortorici, M. A. *et al.* Broad sarbecovirus neutralization by a human monoclonal antibody. *Nature* **597**, 103-108, doi:10.1038/s41586-021-03817-4 (2021).

bioRxiv preprint doi: https://doi.org/10.1101/2021.12.07.470392; this version posted December 22, 2021. The copyright holder for this preprint (which was not certified by peer review) is the author/funder. All rights reserved. No reuse allowed without permission.

36 Dong, J. *et al.* Genetic and structural basis for SARS-CoV-2 variant neutralization by a two-antibody cocktail. *Nat Microbiol* **6**, 1233-1244, doi:10.1038/s41564-021-00972-2 (2021).

37 Starr, T. N. *et al.* SARS-CoV-2 RBD antibodies that maximize breadth and resistance to escape. *Nature* **597**, 97-102, doi:10.1038/s41586-021-03807-6 (2021).

38 Martinez, D. R. *et al.* A broadly cross-reactive antibody neutralizes and protects against sarbecovirus challenge in mice. *Sci Transl Med*, eabj7125, doi:10.1126/scitranslmed.abj7125 (2021).

39 Onodera, T. *et al.* A SARS-CoV-2 antibody broadly neutralizes SARS-related coronaviruses and variants by coordinated recognition of a virus-vulnerable site. *Immunity* **54**, 2385-2398 e2310, doi:10.1016/j.immuni.2021.08.025 (2021).

40 Raybould, M. I. J., Kovaltsuk, A., Marks, C. & Deane, C. M. CoV-AbDab: the coronavirus antibody database. *Bioinformatics* **37**, 734-735, doi:10.1093/bioinformatics/btaa739 (2021).

41 Barnes, C. O. *et al.* Structures of Human Antibodies Bound to SARS-CoV-2 Spike Reveal Common Epitopes and Recurrent Features of Antibodies. *Cell* **182**, 828-842 e816, doi:10.1016/j.cell.2020.06.025 (2020).

42 Hansen, J. *et al.* Studies in humanized mice and convalescent humans yield a SARS-CoV-2 antibody cocktail. *Science* **369**, 1010-1014, doi:10.1126/science.abd0827 (2020).

43 Kim, S. I. *et al.* Stereotypic Neutralizing VH Clonotypes Against SARS-CoV-2 RBD in COVID-19 Patients and the Healthy Population. *bioRxiv*, 2020.2006.2026.174557, doi:10.1101/2020.06.26.174557 (2020).

44 Du, S. *et al.* Structurally Resolved SARS-CoV-2 Antibody Shows High Efficacy in Severely Infected Hamsters and Provides a Potent Cocktail Pairing Strategy. *Cell* **183**, 1013-1023 e1013, doi:10.1016/j.cell.2020.09.035 (2020).

45 Du, S. *et al.* Structures of SARS-CoV-2 B.1.351 neutralizing antibodies provide insights into cocktail design against concerning variants. *Cell Res* **31**, 1130-1133, doi:10.1038/s41422-021-00555-0 (2021).

46 Harvey, W. T. *et al.* SARS-CoV-2 variants, spike mutations and immune escape. *Nat Rev Microbiol* **19**, 409-424, doi:10.1038/s41579-021-00573-0 (2021).

47 Jones, B. E. *et al.* The neutralizing antibody, LY-CoV555, protects against SARS-CoV-2 infection in nonhuman primates. *Sci Transl Med* **13**, doi:10.1126/scitranslmed.abf1906 (2021).

48 Tan, C. W. *et al.* Pan-Sarbecovirus Neutralizing Antibodies in BNT162b2-Immunized SARS-CoV-1 Survivors. *N Engl J Med* **385**, 1401-1406, doi:10.1056/NEJMoa2108453 (2021).

Figure legends

Fig. 1: Omicron greatly reduces the neutralization potency of NAbs of diverse epitopes.

a, Schematic of MACS-based high-throughput yeast display mutation screening. **b,**

bioRxiv preprint doi: https://doi.org/10.1101/2021.12.07.470392; this version posted December 22, 2021. The copyright holder for this preprint (which was not certified by peer review) is the author/funder. All rights reserved. No reuse allowed without permission.

Representative NAb structures of each epitope group. **c,** t-SNE embedding and unsupervised clustering of SARS-CoV-2 human NAbs based on each antibody escaping mutation profile. A total of 6 epitope groups (Group A-F) could be defined. **d,** Neutralization of Omicron variant (spike-pseudotyped VSV) by 247 RBD NAbs. Shades of red show IC50 fold change compared with D614G of each NAb. **e,** Neutralization of SARS-CoV-1 (spike-pseudotyped VSV) by 247 RBD NAbs. Shades of red show the IC50 value (μg/mL) of each NAb. All pseudovirus neutralization assays are conducted in biological duplicates or triplicates.

Fig. 2: The neutralizing abilities of Group A-C NAbs are mostly abolished by Omicron.

a-c, Escaping mutation profiles of representative NAbs for group A-C, respectively. For each site, the height of a letter indicates the detected mutation escape score of its corresponding residue. Sites mutated in Omicron are highlighted. **d-f,** Heatmaps of site escape scores for NAbs of epitope group A-C, respectively. ACE2 interface residues are annotated with red blocks, and mutated sites in Omicron are marked red. Annotations on the right side of heatmaps represent pseudovirus neutralizing IC50 fold change (FC) for Omicron and Beta compared to D614G. **g-i,** Representative structures of group A-C antibodies in complex with RBD. Residues involved in important contacts are labeled. Omicron mutations are marked as blue. NAb escaping mutations (Omicron) inferred from yeast display are labeled with squares.

Fig. 3: The majority of Group D-E NAbs are escaped by Omicron.

a-c, Escaping mutation profiles of representative NAbs for group D-E, respectively. For each site, the height of a letter indicates the detected mutation escape score of its corresponding residue. Sites mutated in Omicron are highlighted. **d-f,** Heatmaps of site escape scores for NAbs of epitope group D-E, respectively. ACE2 interface residues are annotated with red blocks, and mutated sites in Omicron are marked red. Annotations on the right side of heatmaps represent pseudovirus neutralizing IC50 fold change (FC) for Omicron and Beta compared to D614G. **g-j,** Representative structures of group D-E antibodies in complex with RBD. Residues involved in important contacts are labeled. Omicron mutations are marked as blue. NAb escaping mutations (Omicron) inferred from yeast display are labeled with squares.

bioRxiv preprint doi: https://doi.org/10.1101/2021.12.07.470392; this version posted December 22, 2021. The copyright holder for this preprint (which was not certified by peer review) is the author/funder. All rights reserved. No reuse allowed without permission.

Fig. 4: Omicron escapes most NAb drugs.

a, Neutralization of SARS-CoV-2 variants of concern (pseudotyped VSV) by 9 NAb drugs. The pseudovirus neutralization assays for every VOC were performed in biological triplicates. IC50 labeled is the average of three replicates shown in Extended Data Fig. 9. **b**, The sarbecovirus neutralization and binding capability of selected potent Omicron-neutralizing antibodies. Monoclonal antibody HG1K (IgG1 antibody against Influenza A virus subtype H7N9) was used as the negative control.

Methods

Human peripheral blood mononuclear cells isolation

SARS-CoV-2 convalescents, SARS-CoV-1 convalescents, and SARS-CoV-2 vaccinees were recruited on the basis of prior SARS-CoV-2 infection or SARS-CoV-1 infection or SARS-CoV-2 at Beijing Youan and Ditan hospital. Relevant experiments regarding SARS-CoV-2 convalescents and vaccinees were approved by the Beijing Youan Hospital Research Ethics Committee (Ethics committee archiving No. LL-2020-010-K). Relevant experiments regarding SARS-CoV-1 convalescents were approved by the Beijing Ditan Hospital Capital Medical University (Ethics committee archiving No. LL-2021-024-02). All participants provided written informed consent for the collection of information, and that their clinical samples were stored and used for research. Data generated from the research were agreed to be published. The detailed information of SARS-CoV-2 convalescents and vaccinees was previously described [11]. Briefly, short-term convalescents' blood samples were obtained at day 62 on average after symptoms onset. Long-term convalescents' blood samples were obtained at day 371 on average after symptoms onset. No vaccination was received before blood collection. SARS-CoV-2 vaccinees' blood samples were obtained 2 weeks after complete vaccination of ZF2001 (RBD-subunit vaccine). For vaccinated SARS-CoV-1 convalescents (average age 58, n = 21), all recruited participants were previously identified for SARS-CoV-1 infection in 2003, and received two-dose vaccination of CoronaVac and a booster dose of ZF2001 with a 180-day-interval. 20mL of blood samples of the vaccinated SARS-CoV-1 convalescents were obtained 2 weeks after the booster shot. Three Healthy vaccinated donor (average age 25) were also included to serve as negative control for FACS gating. Peripheral Blood Mononuclear Cells (PBMCs) were separated from whole blood samples based on the detailed protocol

bioRxiv preprint doi: https://doi.org/10.1101/2021.12.07.470392; this version posted December 22, 2021. The copyright holder for this preprint (which was not certified by peer review) is the author/funder. All rights reserved. No reuse allowed without permission.

described previously [11]. Briefly, blood samples were first diluted with 2% Fetal Bovine Serum (FBS) (Gibco) in Phosphate Buffer Saline (PBS) (Invitrogen) and subjected to Ficoll (Cytiva) gradient centrifugation. After red blood cell lysis and washing steps, PBMCs were resuspended with 2% FBS in PBS for downstream B cell isolation or 10% Dimethyl sulfoxide (Sigma-Aldrich) in FBS for further preservation.

Antigen-specific B cell sorting and sequencing

Starting with freshly isolated or thawed PBMCs, B cells were enriched by positive selection using a CD19+ B cell isolation kit according to the manufacturer's instructions (STEMCELL). The enriched B cells were stained in FACS buffer (1× PBS, 2% FBS, 1 mM EDTA) with the following anti-human antibodies and antigens: For every 10^6 cells, 3 μL FITC anti-CD19 Antibody (Biolegend, 392508), 3 μL FITC anti-CD20 Antibody (Biolegend, 302304), 3.5 μL Brilliant Violet 421 anti-CD27 Antibody (Biolegend, 302824), 3 μL PE/Cyanine7 anti-IgM(Biolegend, 314532), and fluorophore-labelled Receptor-Binding Domain (RBD) and ovalbumin (Ova) for 30 min on ice. Cells were stained with 5 μL 7-AAD (eBioscience, 00-6993-50) for 10 minutes before sorting. Biotinylated receptor binding domain (RBD) of SARS (Sino biological, 40634-V27H-B) or SARS-CoV-2 (Sino biological, 40592-V27H-B) were multimerized with fluorescently labeled Streptavidin (SA) for 1 hour at 4°C. RBD was mixed with SA-PE (Biolegend, 405204) and SA-APC (Biolegend, 405207) at a 4:1 molar ratio. For every 10^6 cells, 6 ng SA was used to stain. Single CD19 or CD20+, CD27+, IgM-, Ova-, RBD-PE+, RBD-APC+, live B cells were sorted on an Astrios EQ (BeckMan Coulter) into PBS containing 30% FBS (Supplementary Data 2). FACS sorting were controlled by Summit 6.0 (Beckman Coulter). FACS data analyses were done by FlowJo 10.8. Cells obtained after FACS were sent for 5′-mRNA and V(D)J libraries preparation as previously described[11], which were further submitted to Illumina sequencing on a Hiseq 2500 platform, with the 26x91 pair-end reading mode.

V(D)J sequence data analysis

The raw FASTQ files were processed by Cell Ranger (version 6.1.1) pipeline using GRCh38 reference. Sequences were generated using "cellranger multi" or "cellranger vdj" with default parameters. Antibody sequences were processed by IMGT/DomainGapAlign (version 4.10.2) to obtain the annotations of V(D)J, regions

bioRxiv preprint doi: https://doi.org/10.1101/2021.12.07.470392; this version posted December 22, 2021. The copyright holder for this preprint (which was not certified by peer review) is the author/funder. All rights reserved. No reuse allowed without permission.

of complementarity determining regions (CDR), and the mutation frequency[49,50]. Mutation count divided by the length of the V gene peptide is defined as the amino acid mutation rate of the V gene.

Recombinant antibody production

Paired immunoglobulin heavy and light chain genes obtained from 10X Genomics V(D)J sequencing and analysis were submitted to recombinant monoclonal antibody synthesis. Briefly, heavy and light genes were cloned into expression vectors, respectively, based on Gibson assembly, and subsequently co-transfected into HEK293F cells (ThermoFisher, R79007). The secreted monoclonal antibodies from cultured cells were purified by protein A affinity chromatography. The specificities of these antibodies were determined by ELISA.

ELISA

ELISA plates were coated with RBD (SARS-CoV-2 WT, SARS-CoV-2 Omicron, SARS-CoV-1 RBD, Sino Biological Inc.) at 0.03 μg/mL and 1 μg/mL in PBS at 4°C overnight. After standard washing and blocking, 100 μL 1μg/mL antibodies were added to each well. After a 2 h incubation at room temperature, plates were washed and incubated with 0.08 μg/mL goat anti-human IgG (H+L)/HRP (JACKSON, 109-035-003) for 1 h incubation at room temperature. Tetramethylbenzidine (TMB) (Solarbio) was then added, and the reaction was stopped by adding H_2SO_4. OD450 was measured by an ELISA microplate reader. An antibody is defined as ELISA-positive when the OD450 (1 μg/mL RBD) is three times larger than the negative control, which utilizes an H7N9 specific human IgG1 antibody (HG1K, Sino Biology Cat #HG1K).

Peudovirus neutralization assay

Pesudovisurs neutralization assay was performed to evaluate neutralizing ability of antibodies. The detailed process was previously described by Cao et al.[12]. Briefly, serially diluted antibodies were first incubated with pseudotyped virus for 1h, and the mixture was then incubated with Huh-7 cells. After 24h incubation in an incubator at 37°C, cells were collected and lysed with luciferase substrate (PerkinElmer), then proceeded to luminescence intensity measurement by a microplate reader. IC50 was

bioRxiv preprint doi: https://doi.org/10.1101/2021.12.07.470392; this version posted December 22, 2021. The copyright holder for this preprint (which was not certified by peer review) is the author/funder. All rights reserved. No reuse allowed without permission.

538 determined by a four-parameter non-linear regression model using PRISM (v9.0.1).
539 Omicron pseudovirus contains the following mutations: A67V, H69del, V70del, T95I,
540 G142D, V143del, Y144del, Y145del, N211del, L212I, ins214EPE, G339D, S371L,
541 S373P, S375F, K417N, N440K, G446S, S477N, T478K, E484A, Q493R, G496S,
542 Q498R, N501Y, Y505H, T547K, D614G, H655Y, N679K, P681H, N764K, D796Y,
543 N856K, Q954H, N969K, L981F.
544

545 **Biolayer interferometry**

546 Biolayer interferometry assays were conducted on Octet® R8 Protein Analysis System
547 (Fortebio) following the manufacturer's instruction. Briefly, after baseline calibration,
548 Protein A biosensors (Fortebio) were immersed with antibodies to capture the antibody,
549 then sensors were immersed in PBS with 0.05% Tween-20 to the baseline. After
550 association with different concentrations of RBD of SARS-CoV-2 variants (Omicron
551 RBD: 40592-V08H85), disassociation was conducted. Data were recorded using Octet
552 BLI Discovery (12.2) and analyzed using Octet BLI Analysis (12.2).
553

554 **RBD Deep Mutational Scanning Library construction**

555 The yeast-display RBD mutant libraries used here were constructed as described by
556 Starr et al.,[12] based on the spike receptor-binding domain (RBD) from SARS-CoV-2
557 (NCBI GenBank: MN908947, residues N331-T531) with the modifications that instead
558 of 16-neuclotide barcode (N16), a unique 26-neuclotide (N26), barcode was appended
559 to each RBD variant as an identifier in order to decrease sequencing cost by eliminating
560 the use of PhiX. Briefly, three rounds of mutagenesis PCR were performed with
561 designed and synthesized mutagenetic primer pools; in order to solid our conclusion,
562 we constructed two RBD mutant libraries independently. RBD mutant libraries were
563 then cloned into pETcon 2649 vector and the assembled products were electroporated
564 into electrocompetent DH10B cells to enlarge plasmid yield. Plasmid extracted form E.
565 coli were transformed into the EBY100 strain of *Saccharomyces cerevisiae* via the
566 method described by Gietz and Schiestl[51]. Transformed yeast population were screened
567 on SD-CAA selective plate and further cultured in SD-CAA liquid medium at a large
568 scale. The resulted yeast libraries were flash frozen by liquid nitrogen and preserved at
569 -80℃.
570

bioRxiv preprint doi: https://doi.org/10.1101/2021.12.07.470392; this version posted December 22, 2021. The copyright holder for this preprint (which was not certified by peer review) is the author/funder. All rights reserved. No reuse allowed without permission.

571 **PacBio library preparation, sequencing, and analysis**

572 The correspondence of RBD gene sequence in mutant library and N26 barcode was
573 obtained by PacBio sequencing. Firstly, the bacterially-extracted plasmid pools were
574 digested by NotI restriction enzyme and purified by agarose gel electrophoresis, then
575 proceed to SMRTbell ligation. Four RBD mutant libraries were sequenced in one
576 SMRT cell on a PacBio Sequel ll platform. PacBio SMRT sequencing subreads were
577 converted to HiFi ccs reads with pbccs, and then processed with a slightly modified
578 version of the script previously described[12] to generate the barcode-variant dictionary.
579 To reduce noise, variants containing stop codons or supported by only one ccs read
580 were removed from the dictionary and ignored during further analysis.
581
582 **Magnetic-activated cell sorting (MACS)-based mutation escape profiling**

583 ACE2 binding mutants were sorted based on magnetic beads to eliminate non-
584 functional RBD variants. Briefly, the biotin binder beads (Thermo Fisher) were washed
585 and prepared as the manufacturer's instruction and incubated with biotinylated ACE2
586 protein (Sino Biological Inc.) at room temperature with mild rotation. The ACE2 bound
587 beads were washed twice and resuspend with 0.1% BSA buffer (PBS supplemented
588 with 0.1% bovine serum albumin), and ready for ACE2 positive selection. Transformed
589 yeast library were inoculated into SD-CAA and grown at 30℃ with shaking for 16-
590 18h, then back-diluted into SG-CAA at 23℃ with shaking to induce RBD surface
591 expression. Yeasts were collected and washed twice with 0.1% BSA buffer and
592 incubated with aforementioned ACE2 bound beads at room temperature for 30min with
593 mild rotating. Then, the bead-bound cells were washed, resuspend with SD-CAA
594 media, and grown at 30℃ with shaking. After overnight growth, the bead-unbound
595 yeasts were separated with a magnet and cultured in a large scale. The above ACE2
596 positive selected yeast libraries were preserved at -80℃ in aliquots as a seed bank for
597 antibody escape mapping.
598
599 One aliquot of ACE2 positive selected RBD library was thawed and inoculated into
600 SD-CAA, then grown at 30℃ with shaking for 16-18h. 120 OD units were back-diluted
601 into SG-CAA media and induced for RBD surface expression. Two rounds of
602 sequential negative selection to sort yeast cells that escape Protein A conjugated
603 antibody binding were performed according to the manufacturer's protocol. Briefly,

bioRxiv preprint doi: https://doi.org/10.1101/2021.12.07.470392; this version posted December 22, 2021. The copyright holder for this preprint (which was not certified by peer review) is the author/funder. All rights reserved. No reuse allowed without permission.

Protein A magnetic beads (Thermo Fisher) were washed and resuspend in PBST (PBS with 0.02% Tween-20). Then beads were incubated with neutralizing antibody and rotated at room temperature for 30min. The antibody-conjugated beads were washed and resuspend in PBST. Induced yeast libraries were washed and incubated with antibody-conjugated beads for 30min at room temperature with agitation. The supernatant was separated and proceed to a second round of negative selection to ensure full depletion of antibody-binding yeast.

To eliminate yeast that did not express RBD, MYC-tag based RBD positive selection was conducted according to the manufacturer's protocol. First, anti-c-Myc magnetic beads (Thermo Fisher) were washed and resuspend with 1X TBST (TBS with Tween-20), then the prepared beads were incubated for 30min with the antibody escaping yeasts after two rounds of negative selection. Yeasts bound by anti-c-Myc magnetic beads were wash with 1X TBST and grown overnight in SD-CAA to expand yeast population prior to plasmid extraction.

Overnight cultures of MACS sorted antibody-escaped and ACE2 preselected yeast populations were proceed to yeast plasmid extraction kit (Zymo Research). PCRs were performed to amplify the N26 barcode sequences as previously described[13]. The PCR products were purified with 0.9X Ampure XP beads (Beckman Coulter) and submitted to 75bp single-end Illumina Nextseq 500 sequencing.

Deep mutational scanning data processing

Raw single-end Illumina sequencing reads were trimmed and aligned to the reference barcode-variant dictionary generated as described above to get the count of each variant with *dms_variants* Python package (version 0.8.9). For libraries with N26 barcodes, we slightly modified the *illuminabarcodeparser* class of this package to tolerate one low sequencing quality base in the barcode region. The escape score of variant X is defined as $F \times (n_{X,ab} / N_{ab}) / (n_{X,ref} / N_{ref})$, where $n_{X,ab}$ and $n_{X,ref}$ is the number of detected barcodes for variant X, N_{ab} and N_{ref} are the total number of barcodes in antibody-selected (ab) library and reference (ref) library respectively as described by Starr et al. [12]. Different from FACS experiments, as we couldn't measure the number of cells retained after MACS selection precisely, here F is considered as a scaling factor to transform raw

bioRxiv preprint doi: https://doi.org/10.1101/2021.12.07.470392; this version posted December 22, 2021. The copyright holder for this preprint (which was not certified by peer review) is the author/funder. All rights reserved. No reuse allowed without permission.

638 escape fraction ratios to 0-1 range, and is calculated from the first and 99th percentiles
639 of raw escape fraction ratios. Scores less than the first percentile or larger than the 99th
640 percentile are considered to be outliers and set to zero or one, respectively. For each
641 experiment, barcodes detected by <6 reads in the reference library were removed to
642 reduce the impact of sampling noise, and variants with ACE2 binding below -2.35 or
643 RBD expression below -1 were removed as previously described [12]. Finally, we built
644 global epistasis models with dms_variants package for each library to estimate single
645 mutation escape scores, utilizing the Python scripts provided by Greaney et al. [16]. To
646 reduce experiment noise, sites are retained for further analysis only if its total escape
647 score is at least 0.01, and at least 3 times greater than the median score of all sites. For
648 antibodies measured by 2 independent experiments, only sites which pass the filter in
649 both experiments are retained. Logo plots in Fig. 2, Fig. 3, Extended Data Fig. 2 and
650 Supplementary Data 1 are generated by Python package *logomaker* (version 0.8).
651

652 **Antibody clustering**

653 Antibody clustering and epitope group identification were performed based on the
654 N×M escape score matrix, where N is the number of antibodies which pass the quality
655 controlling filters, and M is the number of informative sites on SARS-CoV-2 RBD.
656 Each entry of the matrix A_{nm} refers to the total escape score of all kinds of mutations
657 on site m of antibody n. The dissimilarity between two antibodies is defined based on
658 the Pearson's correlation coefficient of their escape score vectors, i. e. D_{ij}=1-
659 Corr($\mathbf{A}_i$,$\mathbf{A}_j$), where Corr($\mathbf{A}_i$, $\mathbf{A}_j$)=$\mathbf{x}_i \cdot \mathbf{x}_j / |\mathbf{x}_i||\mathbf{x}_j|$ and vector $\mathbf{x}_i$=$\mathbf{A}_i$-Mean($\mathbf{A}_i$). Sites with at
660 least 6 escaped antibodies (site escape score >1) were considered informative and
661 selected for dimensionality reduction and clustering. We utilized R function *cmdscale*
662 to convert the cleaned escape matrix into an N×6 feature matrix by multidimensional
663 scaling (MDS) with the dissimilarity metric described above, followed by unsupervised
664 k-medoids clustering within this 6-dimensional antibody feature space, using *pam*
665 function of R package *cluster* (version 2.1.1). Finally, two-dimensional t-Distributed
666 Stochastic Neighbor Embedding (tSNE) embeddings were generated with *Rtsne*
667 package (version 0.15) for visualization. 2D t-SNE plots are generated by *ggplot2*
668 (version 3.3.3), and heatmaps are generated by *ComplexHeatmap* package (version
669 2.6.2).
670

bioRxiv preprint doi: https://doi.org/10.1101/2021.12.07.470392; this version posted December 22, 2021. The copyright holder for this preprint (which was not certified by peer review) is the author/funder. All rights reserved. No reuse allowed without permission.

Reference

49 Ehrenmann, F., Kaas, Q. & Lefranc, M. P. IMGT/3Dstructure-DB and IMGT/DomainGapAlign: a database and a tool for immunoglobulins or antibodies, T cell receptors, MHC, IgSF and MhcSF. *Nucleic Acids Res* **38**, D301-307, doi:10.1093/nar/gkp946 (2010).

50 Ehrenmann, F. & Lefranc, M. P. IMGT/DomainGapAlign: IMGT standardized analysis of amino acid sequences of variable, constant, and groove domains (IG, TR, MH, IgSF, MhSF). *Cold Spring Harb Protoc* **2011**, 737-749, doi:10.1101/pdb.prot5636 (2011).

51 Gietz, R. D. & Schiestl, R. H. High-efficiency yeast transformation using the LiAc/SS carrier DNA/PEG method. *Nat Protoc* **2**, 31-34, doi:10.1038/nprot.2007.13 (2007).

Acknowledgments

We thank Professor Jesse Bloom for his generous gift of the yeast SARS-CoV-2 RBD libraries. We thank Beijing BerryGenomics for the help on DNA sequencing. We thank Sino Biological Inc. for the technical assistance on mAbs and Omicron RBD expression. We thank Sartorius (Shanghai) Trading Co., Ltd. for providing instrumental help with BLI measurement. We thank Jia Luo and Hongxia Lv (National Center for Protein Sciences and core facilities at School of Life Sciences at Peking University) for the help in flow cytometry. This project is financially supported by the Ministry of Science and Technology of China (CPL-1233).

Author contributions

Y.C. and X.S.X designed the study. Y.C. and F.S coordinated the characterizations of the NAbs. J.W., F.J., H.L., H.S. performed and analyzed the yeast display mutation screening experiments. T.X., W.J., X.Y., P.W., H.L. performed the pseudovirus neutralization assays. W.H., Q.L., T.L., Y.Y., Q.C., S.L., Y.W. prepared the VSV-based SARS-CoV-2 pseudovirus. A.Y., Y.W., S.Y., R.A., W.S. performed and analyzed the antigen-specific single B cell VDJ sequencing. X.N., R.A. performed the antibody BLI studies. Z.C., S.D., P.L., L.W., Z.Z., X.W., J.X. performed the antibody structural analyses. P.W., Y.W., J.W, H.S, H.L. performed the ELISA experiments. X.H. and R.J. coordinated the blood samples of vaccinated SARS-CoV-1 convalescents. Y.C., X.W., J.X., X.S.X wrote the manuscript with inputs from all authors.

Declaration of interests

bioRxiv preprint doi: https://doi.org/10.1101/2021.12.07.470392; this version posted December 22, 2021. The copyright holder for this preprint (which was not certified by peer review) is the author/funder. All rights reserved. No reuse allowed without permission.

X.S.X. and Y.C. are inventors on the patent application of DXP-604 and BD series antibodies. X.S.X. and Y.C. are founders of Singlomics Biopharmaceuticals Inc. Other authors declare no competing interests.

Corresponding authors

Correspondence to Yunlong Cao or Xiangxi Wang or Junyu Xiao or Youchun Wang or Xiaoliang Sunney Xie. Request for materials described in this study should be directed to Xiaoliang Sunney Xie.

Data availability

Data availabilityProcessed escape maps for NAbs are available in Supplementary Data 1 (as figures), or at https://github.com/sunneyxielab/SARS-CoV-2-RBD-Abs-HTDMS (as mutation escape score data). Raw Illumina and PacBio sequencing data are available on NCBI Sequence Read Archive BioProject PRJNA787091. We used vdj_GRCh38_alts_ensembl-5.0.0 as the reference of V(D)J alignment, which can be obtained from https://support.10xgenomics.com/single-cell-vdj/software/downloads/latest.
IMGT/DomainGapAlign is based on the built-in lastest IMGT antibody database, and we let the "Species" parameter as "Homo sapiens" while kept the others as default. FACS-based deep mutational scanning datasets could be downloaded from https://media.githubusercontent.com/media/jbloomlab/SARS2_RBD_Ab_escape_maps/main/processed_data/escape_data.csv.
Processed data of this study has been added to this repository as well.

Code availability

Scripts for analyzing SARS-CoV-2 escaping mutation profile data and for reproducing figures in this paper are available at https://github.com/sunneyxielab/SARS-CoV-2-RBD-Abs-HTDMS.

Extended Data Fig. 1: Illustration of SARS-CoV-2 spike with Omicron's mutations.

a, SARS-CoV-2 D614G spike protein structure overlayed with Omicron mutations. Omicron's (BA.1) popular mutations are marked by red (for substitutions), blue (for insertions) and gray balls (for deletions). **b**, NTD-binding NAbs shown together in

bioRxiv preprint doi: https://doi.org/10.1101/2021.12.07.470392; this version posted December 22, 2021. The copyright holder for this preprint (which was not certified by peer review) is the author/funder. All rights reserved. No reuse allowed without permission.

742 complex with NTD. Substitutions and deletions of Omicron NTD are colored blue and
743 red, respectively.
744
745 **Extended Data Fig. 2: Comparison between FACS and MACS-based deep**
746 **mutational scanning.**
747 Deep mutational scanning maps with MACS-based (left) and FACS-based assays
748 (right) of seven therapeutic neutralizing antibodies that have received emergency use
749 authorization. Sites mutated in the Omicron variant are highlighted. Mutation amino
750 acids of each site are shown by single letters. The heights represent mutation escape
751 score, and colors represent chemical properties. FACS-based data were obtained from
752 public datasets by Jesse Bloom.
753
754 **Extended Data Fig. 3: Omicron neutralization IC50 fold-change distribution of**
755 **247 NAbs of diverse epitopes.**
756 Fold-change of IC50 (VSV pseudovirus neutralization) compared to D614G by Beta
757 and Omicron (BA.1) are shown for all 247 NAbs tested. The impact of each RBD
758 mutation of Omicron on NAbs' binding is inferred from yeast display mutation
759 screening. Each NAb's binding to Omicron RBD was validated through ELISA. All
760 neutralization and ELISA assays were conducted in biological duplicates.
761
762 **Extended Data Fig. 4: Heavy chain V/J segment recombination of NAbs of each**
763 **epitope group.**
764 **a-f,** Chord diagrams showing the heavy chain V segment and J segment recombination
765 of epitope group A(a), B(b), C(c), D(d), E(e) and F(f). The width of the arc linking a V
766 segment to a J segment indicates the antibody number of the corresponding
767 recombination. The inner layer scatter plots show the V segment amino acid mutation
768 rate, while black strips show the 25%~75% quantile of mutation rates.
769
770 **Extended Data Fig. 5. Neutralization potency, heavy chain CDR3 length, and**
771 **mutation rate distribution for NAbs of each epitope group.**
772 **a,** The length of H chain complementarity-determining region 3 (HCDR3) amino acid
773 sequence for NAbs in each epitope group (n=66, 26, 57, 27, 39, 32 antibodies for
774 epitope group A, B, C, D, E, F, respectively). HCDR3 lengths are displayed as mean ±
775 s.d. **b,** The V segment amino acid mutation rate for NAbs in each epitope group (n=66,

bioRxiv preprint doi: https://doi.org/10.1101/2021.12.07.470392; this version posted December 22, 2021. The copyright holder for this preprint (which was not certified by peer review) is the author/funder. All rights reserved. No reuse allowed without permission.

776 26, 57, 27, 39, 32 antibodies for epitope group A, B, C, D, E, F, respectively). Mutation
777 rates are calculated are displayed as mean ± s.d. **c-e,** The IC50 against D614G(c),
778 Beta(d), and Omicron(e) variants for NAbs in each epitope group (n=66, 26, 57, 27, 39,
779 32 antibodies for epitope group A, B, C, D, E, F, respectively). IC50 values are
780 displayed as mean ± s.d. in the log10 scale. Pseudovirus assays for each variant are
781 biologically replicated twice. Dotted lines show the detection limit, which is from
782 0.0005 μg/mL to 10 μg/mL. IC50 geometric means are also labeled on the figure.
783
784 **Extended Data Fig. 6: Escape hotspots of different epitope groups on the RBD**
785 **surface.**
786 **a-f,** Aggregated site escape scores of antibodies for epitope group A-F, respectively.
787 Epitope groups are distinguished by distinct colors, and the shades show normalized
788 site escape scores. Escape hotspots of each epitope group are annotated by arrows.
789
790 **Extended Data Fig. 7: Antibody-RBD interface distribution for NAbs of each**
791 **epitope group.**
792 **a-f,** Aggregated antibody-antigen interface of antibodies for epitope group A-F,
793 respectively. Antibody-antigen interface was indicated from publicly available
794 structures of neutralizing antibodies in complex with SARS-CoV-2 RBD. Different
795 colors distinguish epitope groups, and the shade reflects group-specific site popularity
796 to appear on the complex interface. Shared interface residues (Omicron) of each group
797 are annotated.
798
799 **Extended Data Fig. 8: Comparison between mutation escape scores estimated**
800 **from yeast display and neutralization of variants carrying corresponding**
801 **mutations.**
802 **a,** K417N escape scores and corresponding K417N pseudovirus neutralizing IC50 fold
803 change compared to D614G pseudovirus of antibodies within epitope group A. **b,**
804 E484K/E484A escape scores and corresponding E484K pseudovirus neutralizing IC50
805 fold change compared to D614G pseudovirus of antibodies within epitope group C.
806
807 **Extended Data Fig. 9: Pseudovirus neutralization of NAb drugs against SARS-**
808 **CoV-2 variants of concern.**
809 Pseudovirus (VSV-based) assays were performed using Huh-7 cells. Data are collected

bioRxiv preprint doi: https://doi.org/10.1101/2021.12.07.470392; this version posted December 22, 2021. The copyright holder for this preprint (which was not certified by peer review) is the author/funder. All rights reserved. No reuse allowed without permission.

from three biological replicates and represented as mean±s.d.

Extended Data Fig. 10: BLI response between NAb drugs and the RBD of SARS-CoV-2 wildtype, Beta, or Omicron strain.

Antibodies were captured by Protein A sensor. The concentrations of RBD are shown in different colors. Dissociation constant (K_D), association constant (ka), and dissociation rate constant (kd) are labeled. NAbs without binding are marked as "Escaped".

bioRxiv preprint doi: https://doi.org/10.1101/2021.12.07.470392; this version posted December 22, 2021. The copyright holder for this preprint (which was not certified by peer review) is the author/funder. All rights reserved. No reuse allowed without permission.

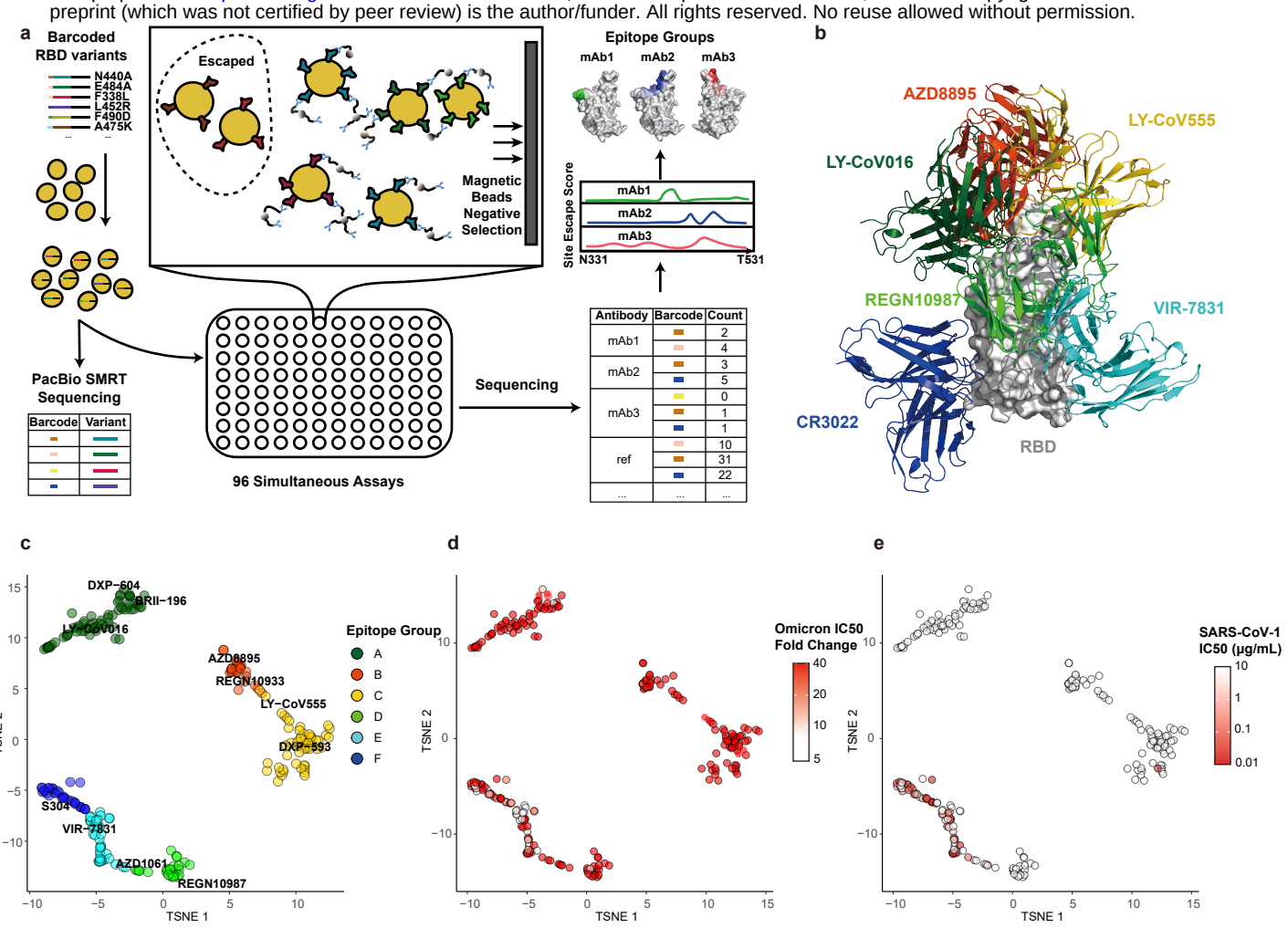

Figure 1

bioRxiv preprint doi: https://doi.org/10.1101/2021.12.07.470392; this version posted December 22, 2021. The copyright holder for this preprint (which was not certified by peer review) is the author/funder. All rights reserved. No reuse allowed without permission.

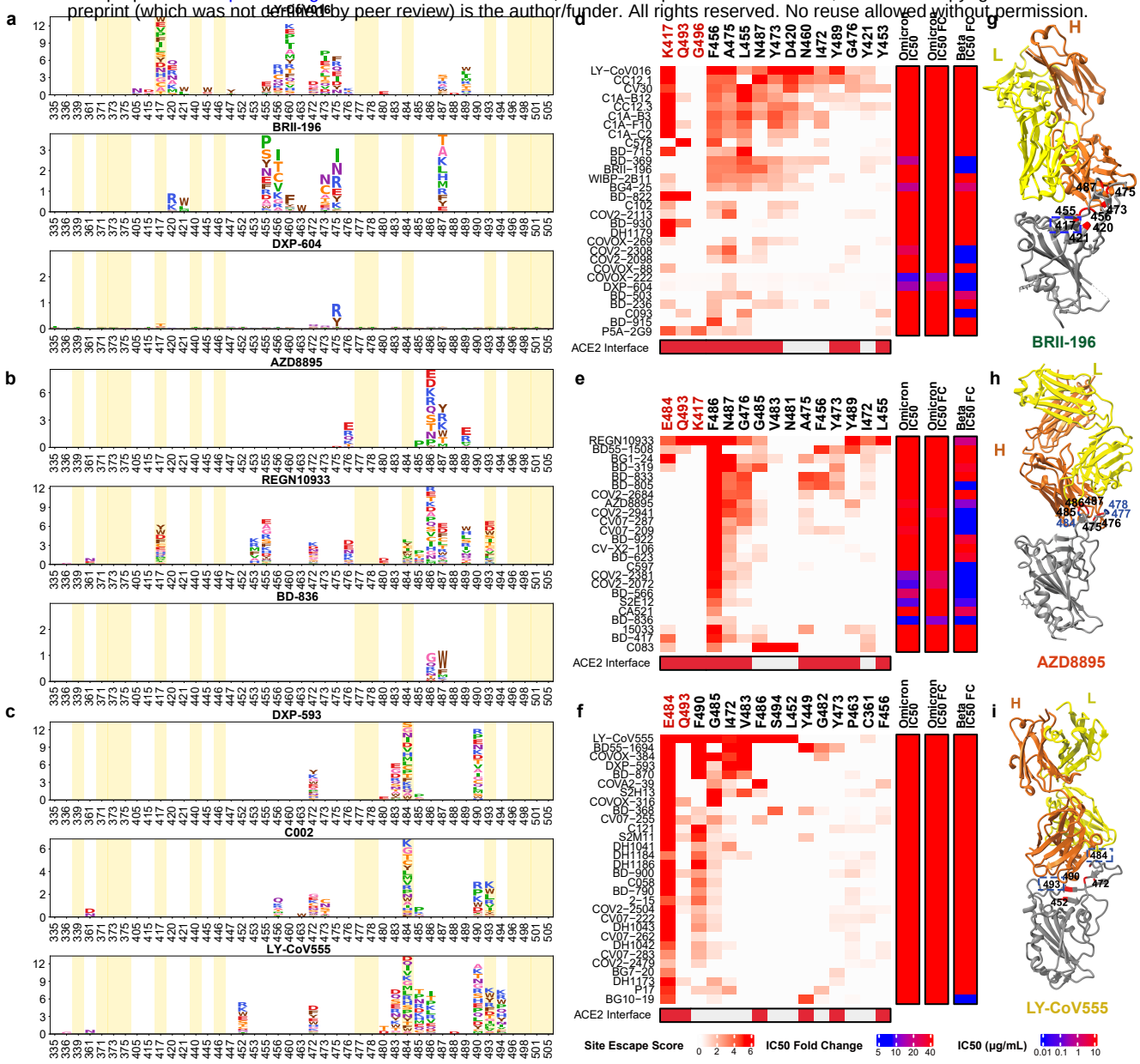

Figure 2

bioRxiv preprint doi: https://doi.org/10.1101/2021.12.07.470392; this version posted December 22, 2021. The copyright holder for this preprint (which was not certified by peer review) is the author/funder. All rights reserved. No reuse allowed without permission.

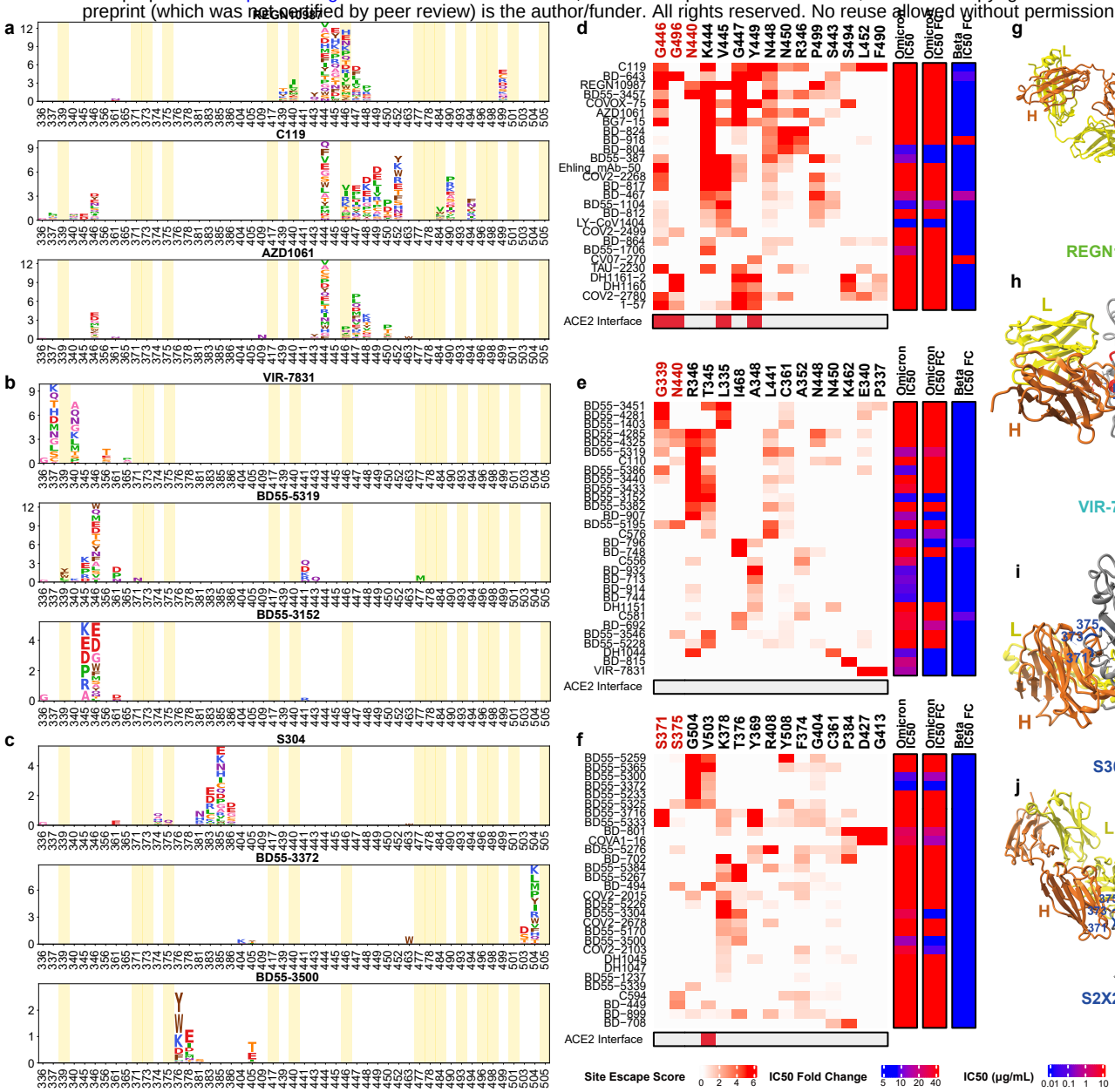

Figure 3

bioRxiv preprint doi: https://doi.org/10.1101/2021.12.07.470392; this version posted December 22, 2021. The copyright holder for this preprint (which was not certified by peer review) is the author/funder. All rights reserved. No reuse allowed without permission.

a

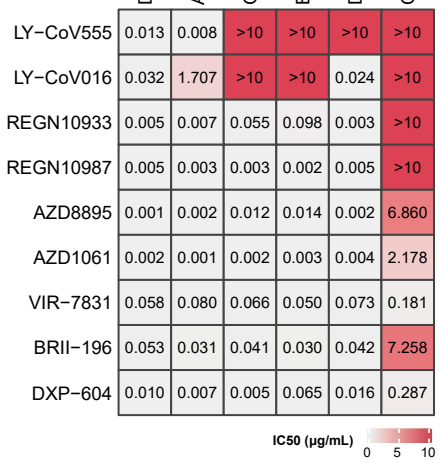

b

Antibody		BD55						HG1K
		3152	5319	5386	5300	3372	3500	
Epitope Group		E	E	E	F	F	F	/
Pseudovirus IC50 (μg/mL)	D614G	0.011	0.015	0.004	0.005	0.007	0.105	>10
	Omicron	0.014	0.369	0.058	0.066	0.010	0.261	>10
	SARS-CoV-1	0.023	0.013	0.009	0.006	0.014	0.052	>10
Sarbecovirus RBD ELISA EC50 (μg/mL)	SARS-CoV-2	SARS-CoV-2	0.009	0.014	0.013	0.018	0.010	0.007	>5
	SARS-CoV-2 clade (1b)	RaTG13	>5	>5	>5	>5	>5	0.008	>5
		Pangolin-GD	0.313	0.126	1.037	0.011	0.009	0.007	>5
		Pangolin-GX	>5	>5	0.377	>5	0.196	0.007	>5
	SARS-CoV-1 clade (1a)	SARS-CoV-1 PC4-127	0.010	0.010	0.010	0.007	0.007	0.006	>5
		SARS-CoV-1 Sin852	0.009	0.011	0.010	0.006	0.006	0.006	>5
		WIV1	0.373	0.771	0.138	0.005	0.005	0.004	>5
	Africa and Europe Clade (3)	BM48-31	>5	0.120	>5	0.020	0.022	0.011	>5
		BtKY72	>5	>5	>5	0.025	0.023	0.020	>5
	Asia non-ACE2-utilizing clade (2)	Shaanxi2011	>5	>5	>5	>5	>5	0.026	>5
		YN2013	>5	>5	>5	>5	>5	0.004	>5

Figure 4

bioRxiv preprint doi: https://doi.org/10.1101/2021.12.07.470392; this version posted December 22, 2021. The copyright holder for this preprint (which was not certified by peer review) is the author/funder. All rights reserved. No reuse allowed without permission.

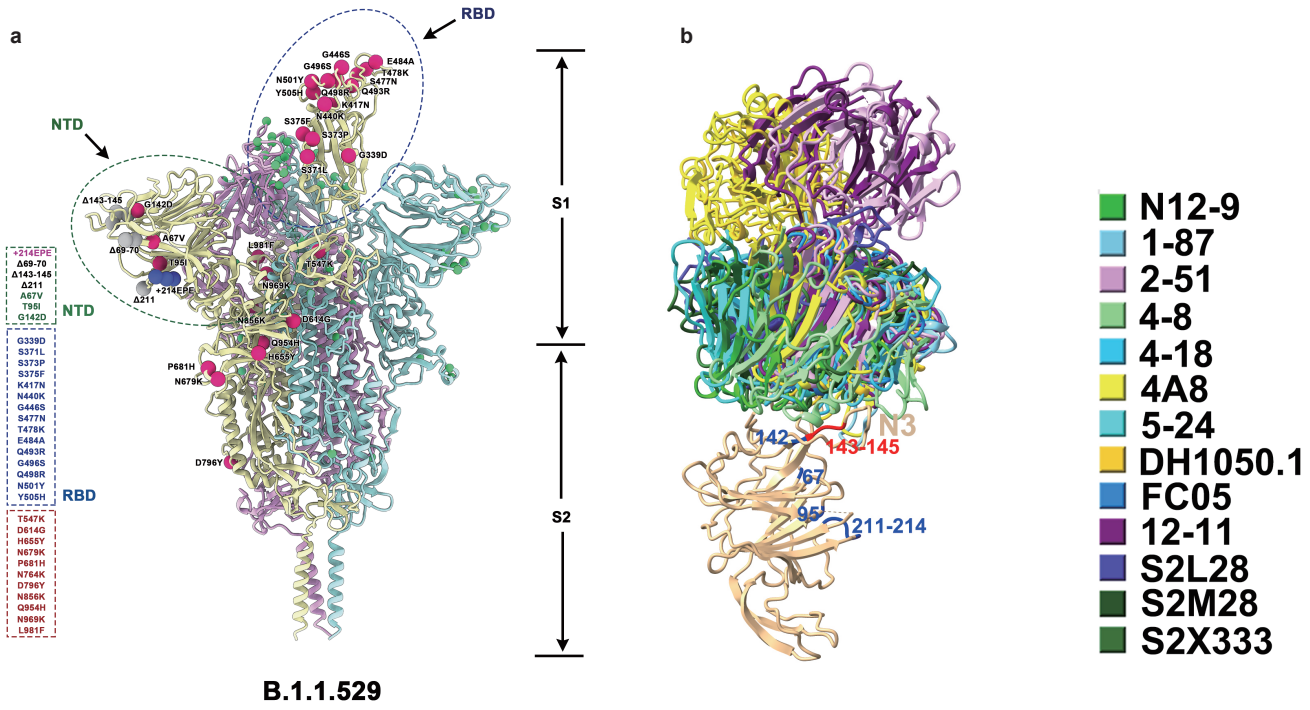

Extended Data Figure 1

bioRxiv preprint doi: https://doi.org/10.1101/2021.12.07.470392; this version posted December 22, 2021. The copyright holder for this preprint (which was not certified by peer review) is the author/funder. All rights reserved. No reuse allowed without permission.

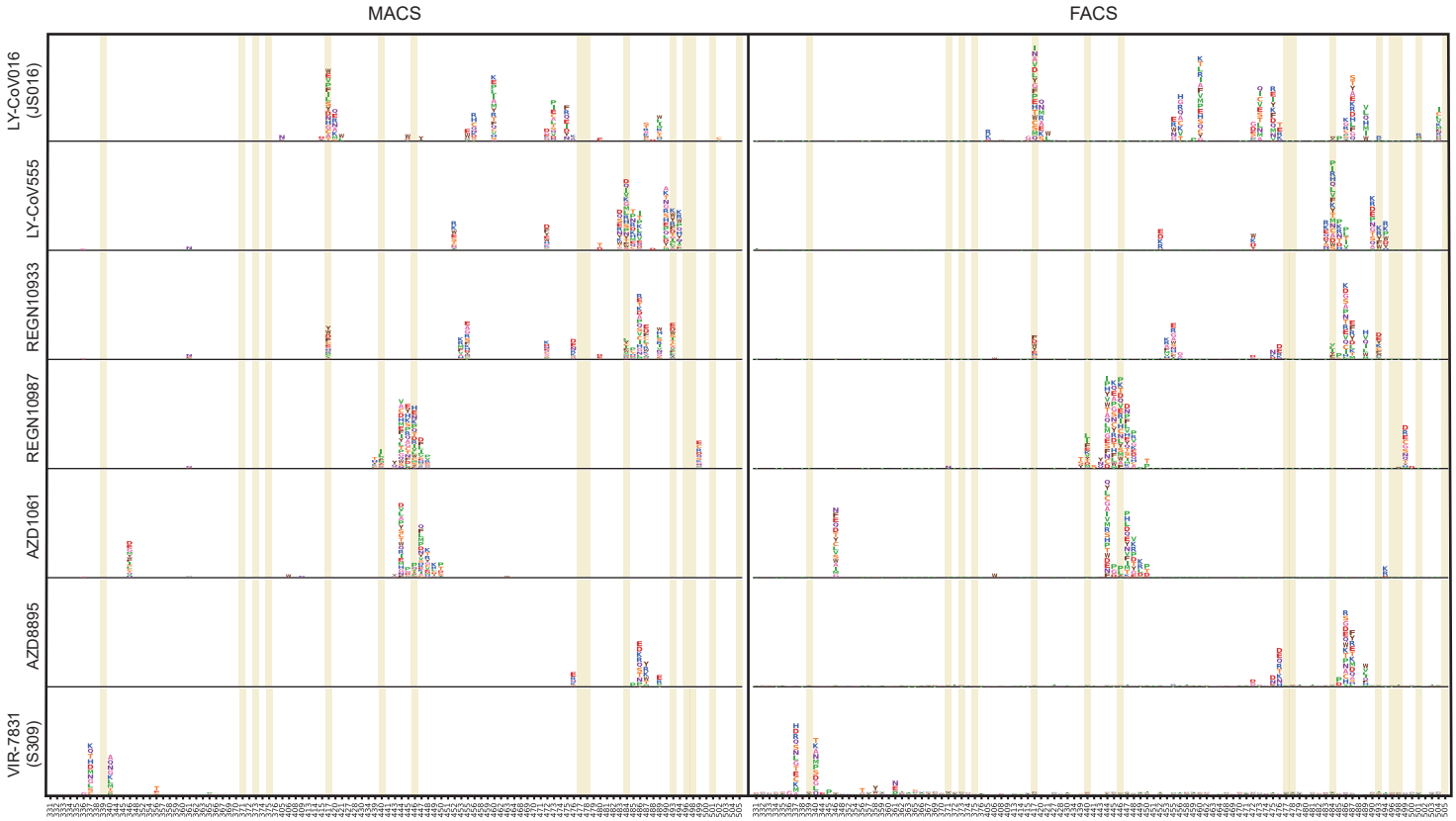

Extended Data Figure 2

bioRxiv preprint doi: https://doi.org/10.1101/2021.12.07.470392; this version posted December 22, 2021. The copyright holder for this preprint (which was not certified by peer review) is the author/funder. All rights reserved. No reuse allowed without permission.

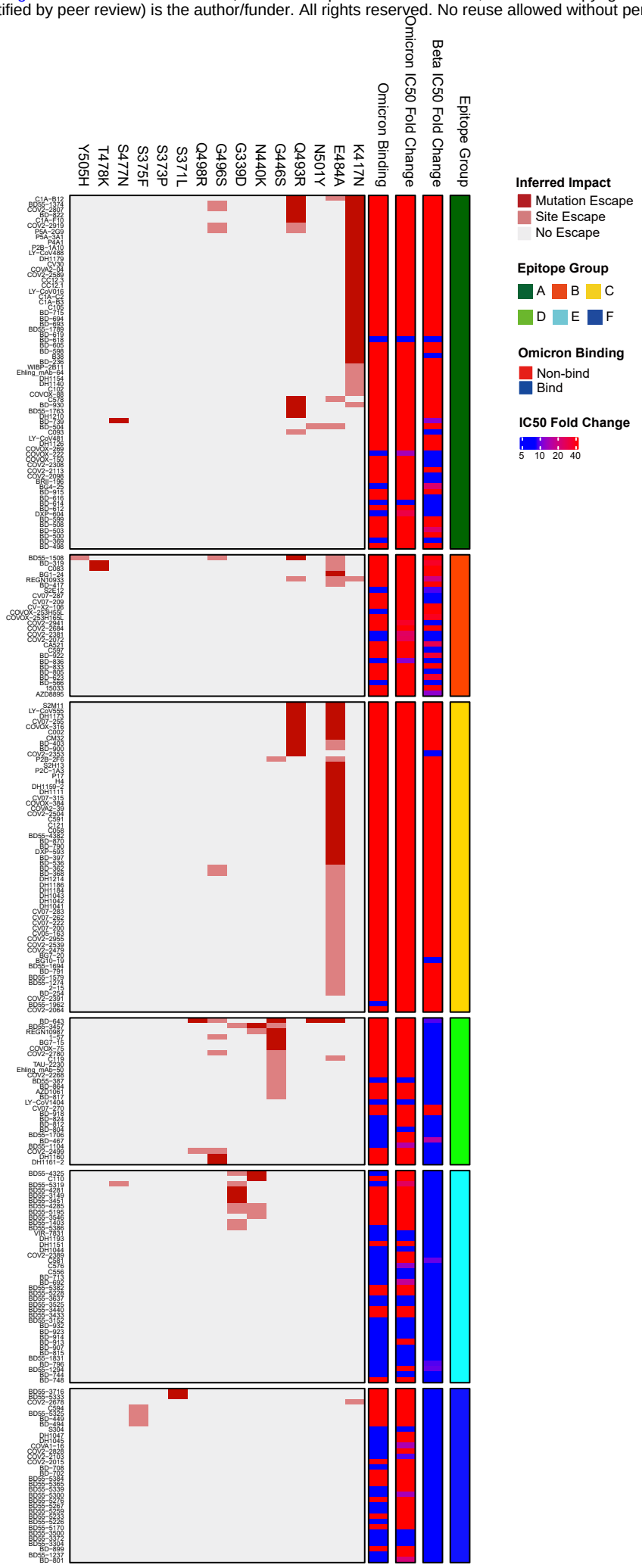

Extended Data Figure 3

bioRxiv preprint doi: https://doi.org/10.1101/2021.12.07.470392; this version posted December 22, 2021. The copyright holder for this preprint (which was not certified by peer review) is the author/funder. All rights reserved. No reuse allowed without permission.

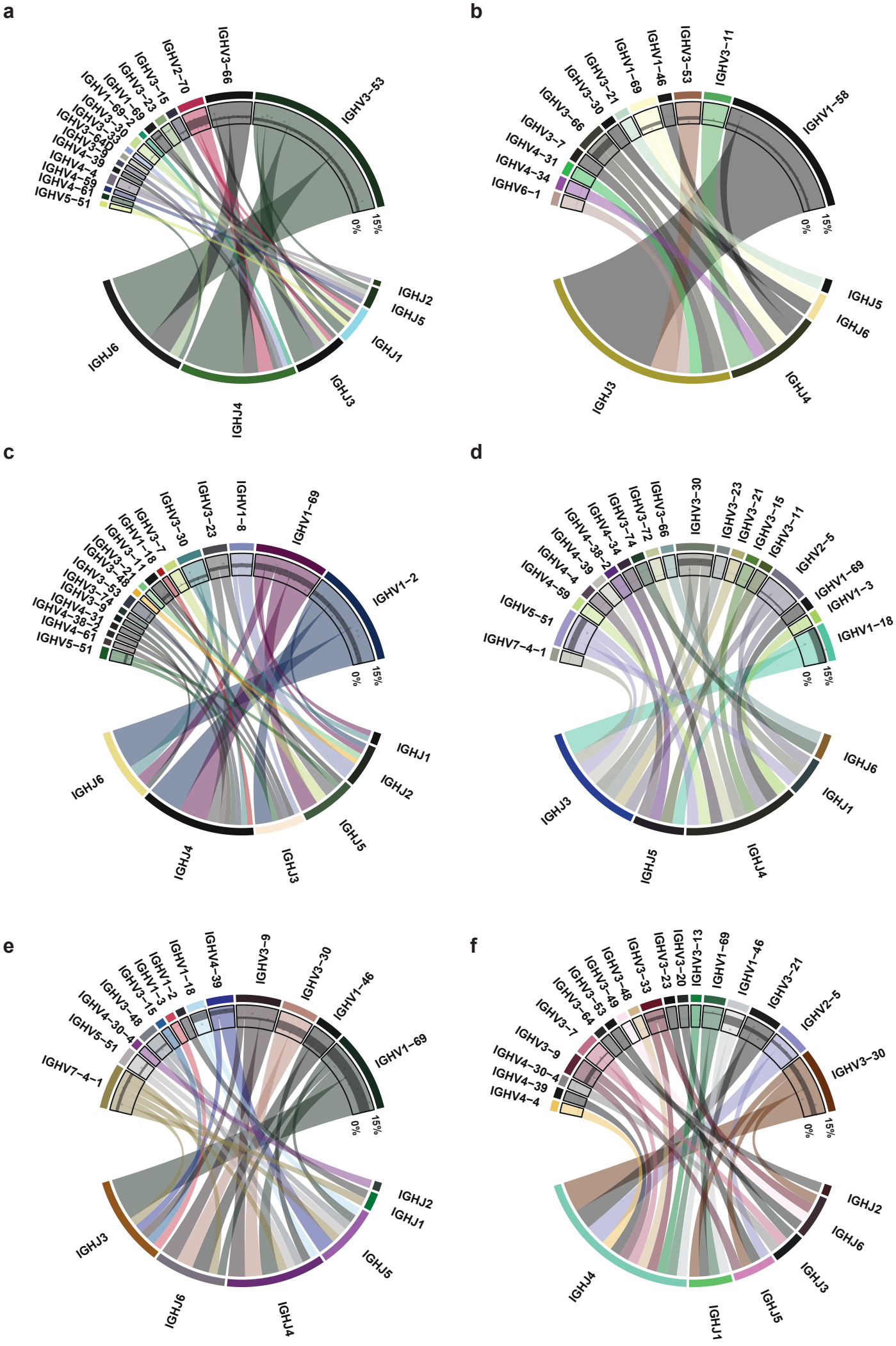

Extended Data Figure 4

bioRxiv preprint doi: https://doi.org/10.1101/2021.12.07.470392; this version posted December 22, 2021. The copyright holder for this preprint (which was not certified by peer review) is the author/funder. All rights reserved. No reuse allowed without permission.

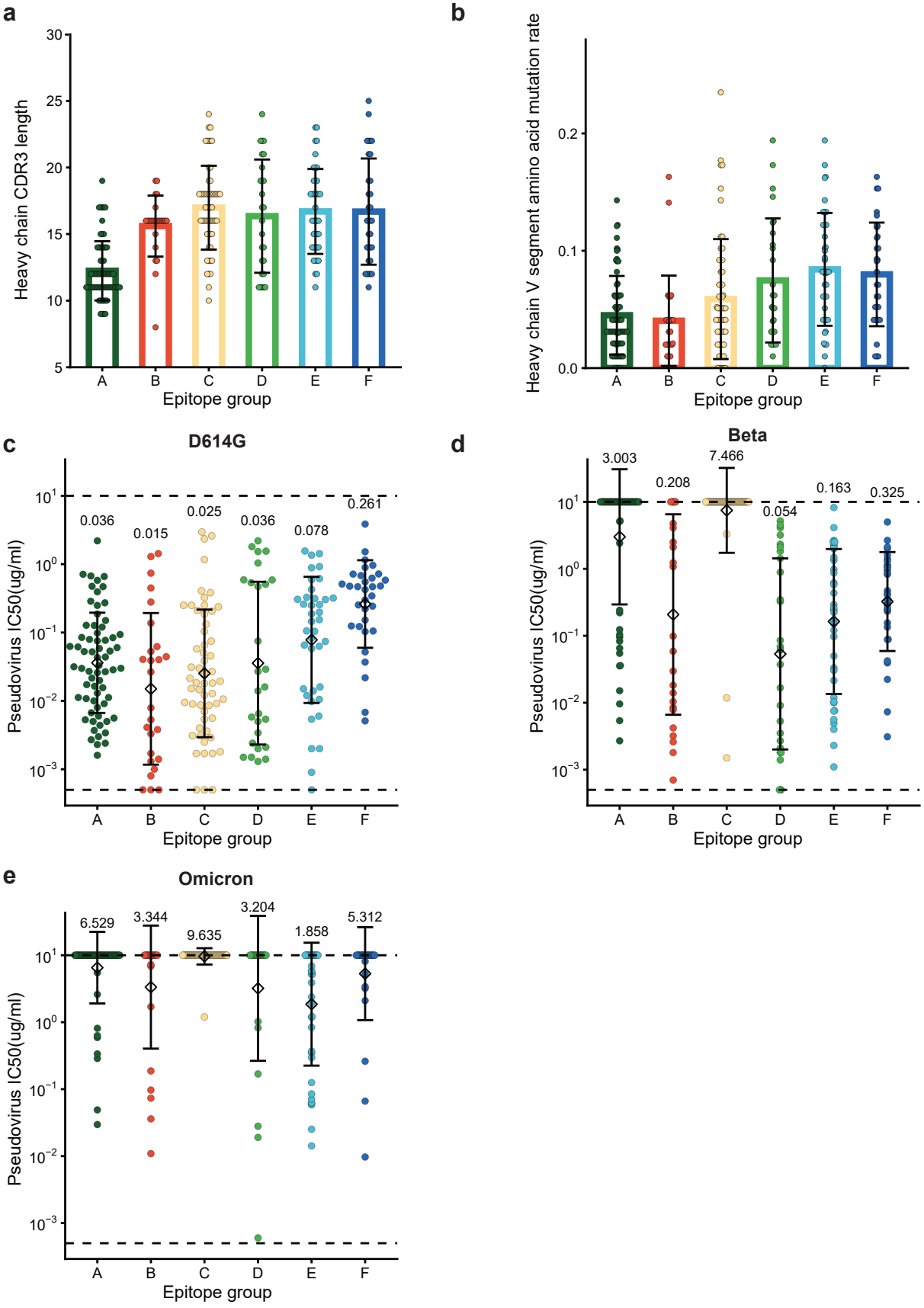

Extended Data Figure 5

bioRxiv preprint doi: https://doi.org/10.1101/2021.12.07.470392; this version posted December 22, 2021. The copyright holder for this preprint (which was not certified by peer review) is the author/funder. All rights reserved. No reuse allowed without permission.

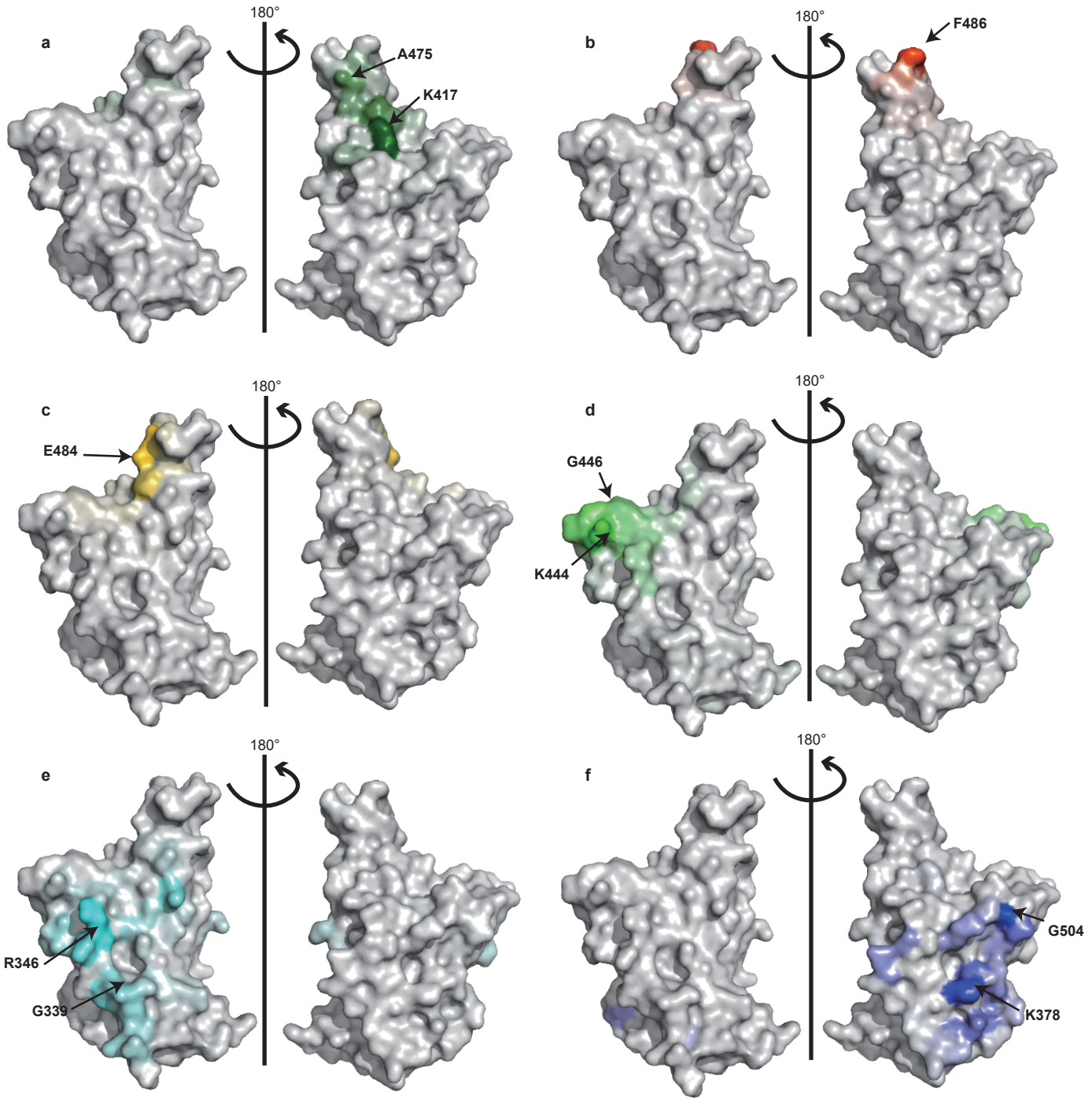

Extended Data Figure 6

bioRxiv preprint doi: https://doi.org/10.1101/2021.12.07.470392; this version posted December 22, 2021. The copyright holder for this preprint (which was not certified by peer review) is the author/funder. All rights reserved. No reuse allowed without permission.

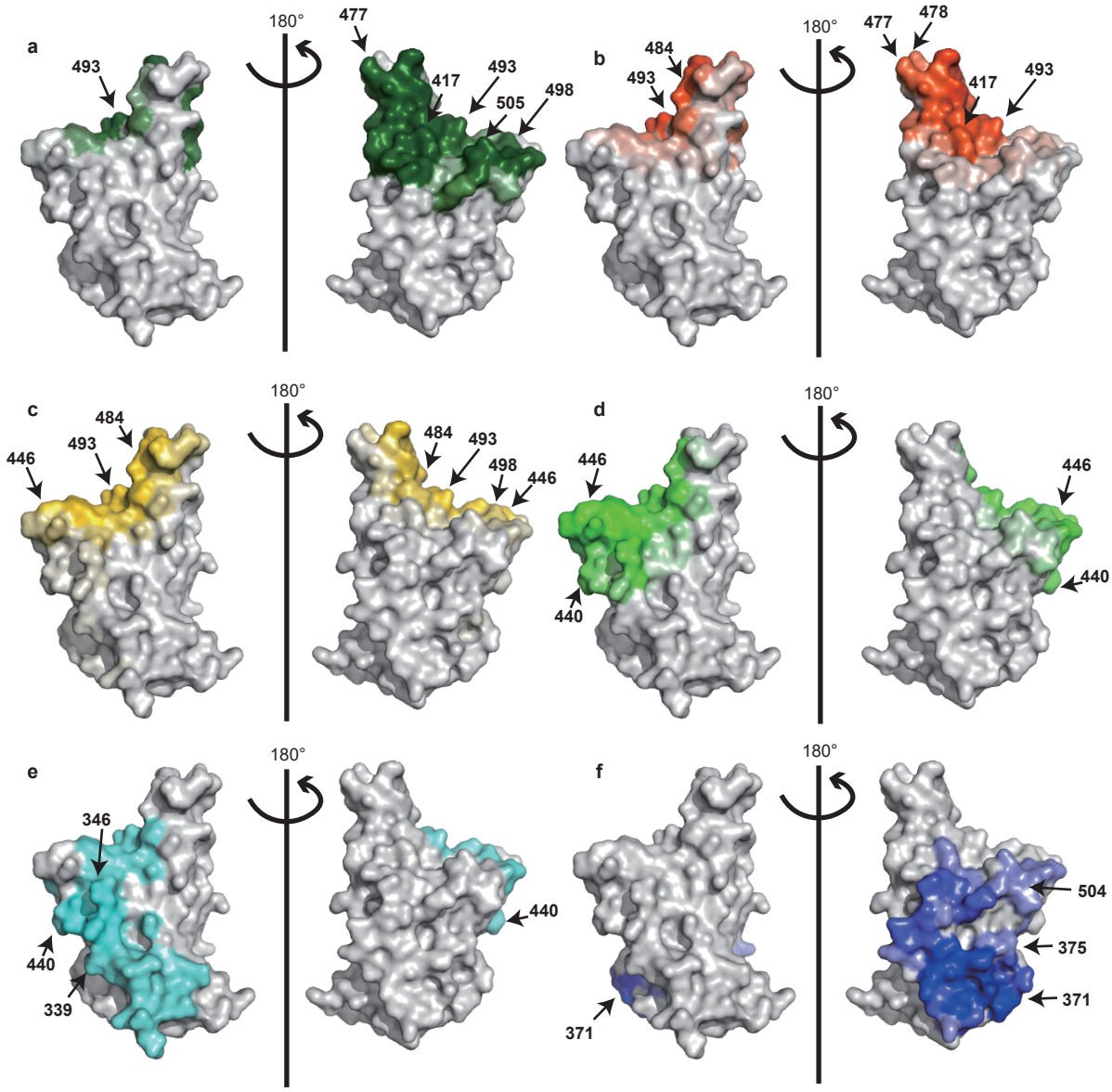

Extended Data Figure 7

bioRxiv preprint doi: https://doi.org/10.1101/2021.12.07.470392; this version posted December 22, 2021. The copyright holder for this preprint (which was not certified by peer review) is the author/funder. All rights reserved. No reuse allowed without permission.

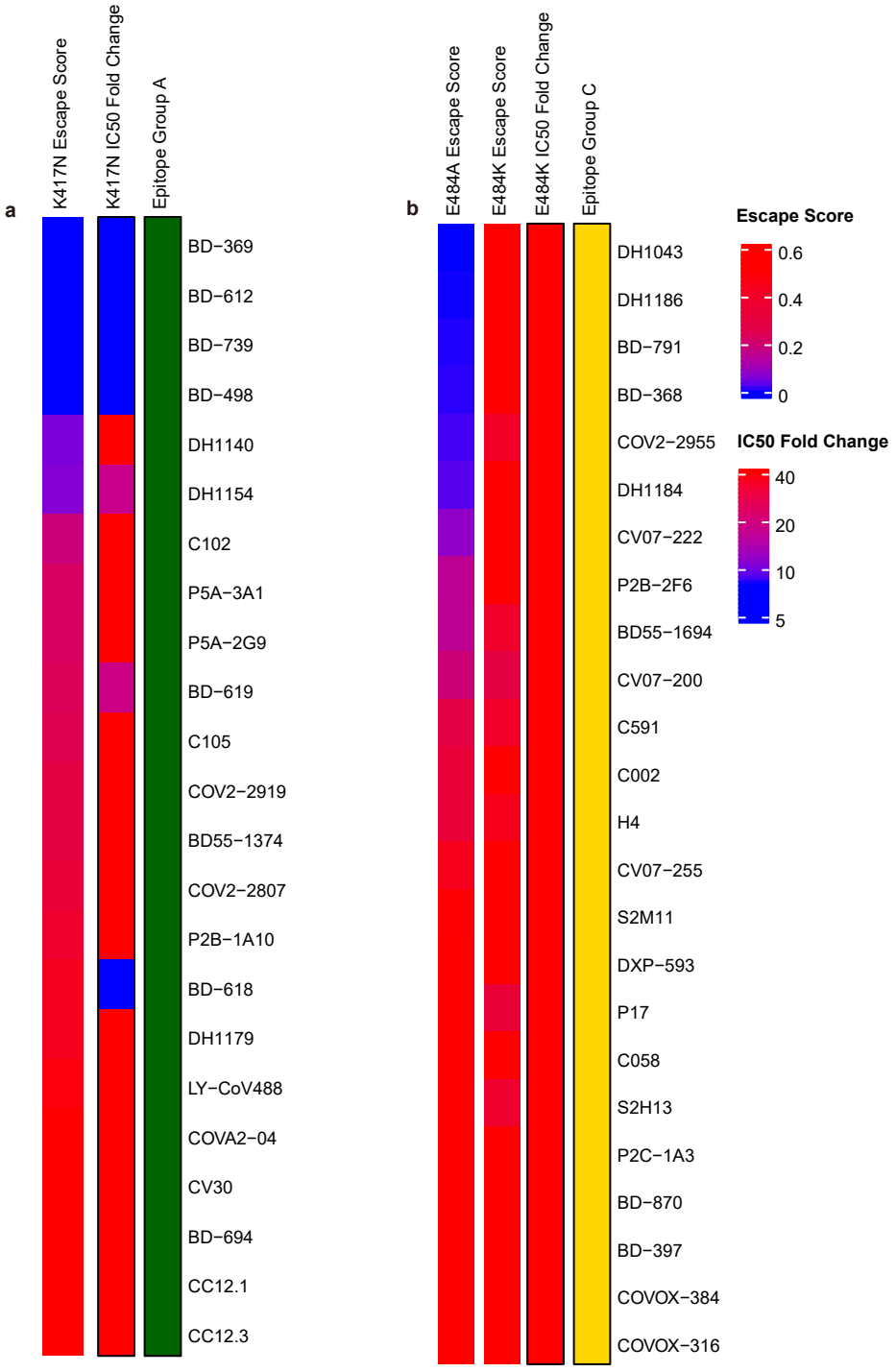

Extended Data Figure 8

bioRxiv preprint doi: https://doi.org/10.1101/2021.12.07.470392; this version posted December 22, 2021. The copyright holder for this preprint (which was not certified by peer review) is the author/funder. All rights reserved. No reuse allowed without permission.

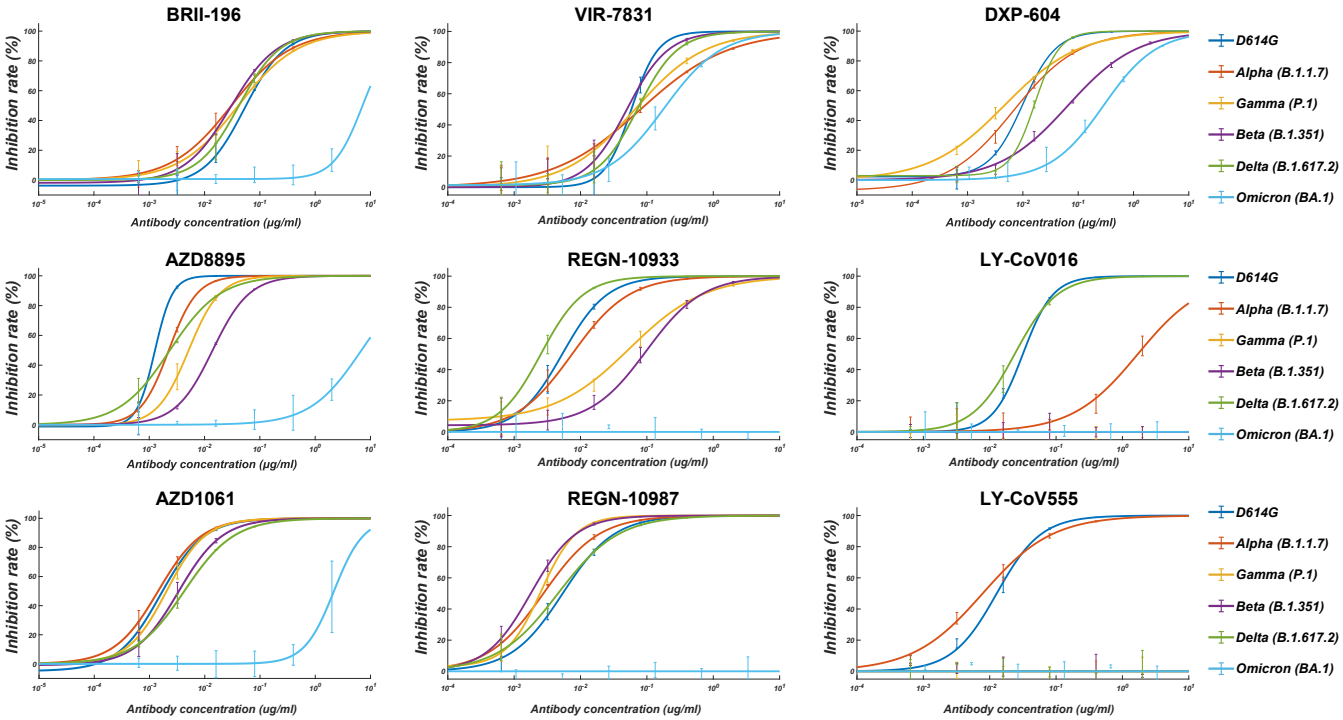

Extended Data Figure 9

bioRxiv preprint doi: https://doi.org/10.1101/2021.12.07.470392; this version posted December 22, 2021. The copyright holder for this preprint (which was not certified by peer review) is the author/funder. All rights reserved. No reuse allowed without permission.

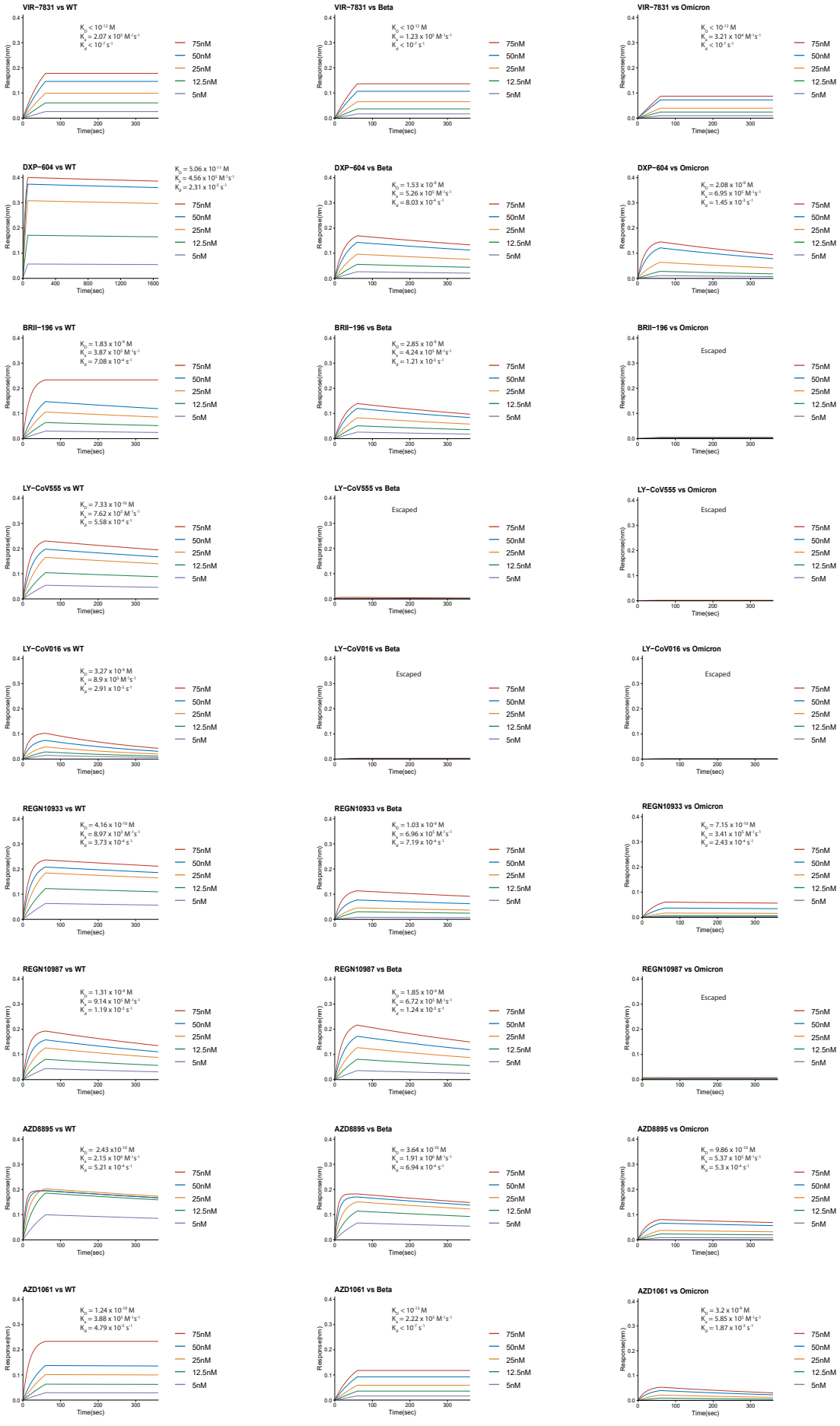

Extended Data Figure 10